1 **Endocrine disruptor-induced epimutagenesis *in vitro*: Insight into molecular mechanisms**

2 Jake D. Lehle, Yu-Huey Lin, Amanda Gomez, Laura Chavez, and John R. McCarrey*

3 Department of Neuroscience, Developmental and Regenerative Biology

4 The University of Texas at San Antonio

5

6 *Corresponding author – John R. McCarrey, john.mccarrey@utsa.edu

7 **Keywords**: Endocrine disrupting chemicals, epigenetics, DNA methylation, epigenetic reprogramming,

8 transgenerational epigenetic inheritance

9

10 **Abstract:**

11 Endocrine disrupting chemicals (EDCs) such as bisphenol S (BPS) are xenobiotic compounds that can

12 disrupt endocrine signaling following exposure due to steric similarities to endogenous hormones within

13 the body. EDCs have been shown to induce disruptions in normal epigenetic programming

14 (epimutations) that accompany dysregulation of normal gene expression patterns that appear to

15 predispose disease states. Most interestingly, the prevalence of epimutations following exposure to

16 many different EDCs often persists over multiple subsequent generations, even with no further

17 exposure to the causative EDC. Many previous studies have described both the direct and prolonged

18 effects of EDC exposure in animal models, but many questions remain about molecular mechanisms by

19 which EDCs initially induce epimutations or contribute to the propagation of EDC-induced epimutations

20 either within the exposed generation or to subsequent generations. Additional questions remain

21 regarding the extent to which there may be differences in cell type-specific susceptibilities to various

22 EDCs, and whether this susceptibility is correlative with expression of relevant hormone receptors

and/or the location of relevant hormone response elements (HREs) in the genome. To address these questions, we exposed cultured mouse pluripotent (induced pluripotent stem [iPS]), somatic (Sertoli and granulosa), and germ (primordial germ cell like [PGCLCs]) cells to BPS and measured changes in DNA methylation levels at the epigenomic level and gene expression at the transcriptomic level. We found that there was indeed a difference in cell type-specific susceptibility to EDC-induced epimutagenesis and that this susceptibility correlated with differential expression of relevant hormone receptors and, in many cases, tended to generate epimutations near relevant HREs within the genome. Additionally, however, we also found that BPS can induce epimutations in a cell type that does not express relevant receptors and in genomic regions that do not contain relevant HREs, suggesting that both canonical and non-canonical signaling mechanisms can be disrupted by BPS exposure. Most interestingly, we found that when iPS cells were exposed to BPS and then induced to differentiate into PGCLCs, the prevalence of epimutations and differentially expressed genes (DEGs) initially induced in the iPSCs was largely retained in the resulting PGCLCs, however, >90% of the specific epimutations and DEGs were not conserved but were rather replaced by novel epimutations and DEGs following the iPSC to PGCLC transition. These results suggest a unique mechanism by which an EDC-induced epimutated state may be propagated transgenerationally following a single exposure to the causative EDC.

Introduction

It has now been more than a half-century since Roy Hertz in 1958 first proposed the notion that certain chemicals, particularly those used in livestock feed at the time, could contaminate food sources and bioaccumulate in humans mimicking the activity of hormones (Gassner et al., 1958). As the number of potential chemicals that could exert these effects has grown, so too has the interest in this area to the point that this is now a major topic of active research. The dangers of many endocrine disrupting

46 chemicals (EDCs) studied to date have largely been investigated utilizing animal models. A primary
47 example is the multi-phased Toxicant Exposures and Responses by Genomic and Epigenomic Regulators
48 of Transcription (TaRGET) program established to determine the contribution of environmental
49 exposures to disease pathogenesis as a function of epigenome perturbation in mouse models (Wang et
50 al., 2018). While the use of animal models has been quite informative for determining the various
51 systemic or organ/tissue-specific disease-related effects associated with exposure to different EDCs, the
52 molecular mechanisms underlying these phenomena remain poorly understood. Thus, questions persist
53 regarding i) the mechanisms by which exposure of cells to EDCs results in the initial formation of
54 epimutations defined here as any change in epigenomic programming, ii) potential cell type-specific
55 differential susceptibility to epimutagenesis induced by different EDCs, iii) the potential involvement of
56 relevant hormone receptors and/or genomic hormone response elements in EDC-induced disruption of
57 the epigenome, and iv) the ability of an EDC-induced epimutated state to persist inter- or
58 transgenerationally despite generational epigenetic reprogramming (Diaz-Castillo et al., 2019).

59 Questions about molecular mechanisms responsible for EDC exposure-based disruption of
60 normal epigenetic programming have been difficult to interpret in whole animal models due, in part, to
61 the inherent complexity of the intact animal including potential interactions among multiple different
62 organs, tissues, and cell types at the paracrine, metabolic and/or systemic levels. To circumvent this
63 challenge, we opted to expose homogeneous populations of specific cell types in culture to doses of the
64 EDC, BPS, that are below the maximum safe limit previously set by the EPA for the similar estrogen
65 mimetic, BPA. In this way we hoped to learn more about the manner in which direct exposure to a
66 specific EDC induces epimutations and differential gene expression in different individual cell types
67 including somatic cells, pluripotent cells, and germ cells. This approach was designed to distinguish the
68 direct effects of an EDC exposure *in vitro* from indirect effects that may accrue as the result of an EDC
69 exposure on one cell type inducing a secondary effect on a neighboring or related cell type *in vivo*.

70 Previous *in vitro* studies have demonstrated direct susceptibility of cultured cell types to EDC-
71 induced epimutagenesis, however, those studies were focused on immortalized cancer cell lines that do
72 not model key cell types involved in normal initial incursion or subsequent intragenerational
73 propagation or inter- or transgenerational transmission of environmentally-induced epimutations *in vivo*
74 (Deb et al., 2016; Goodman et al., 2014; Huang et al., 2019; Karaman and Ozden, 2019; Senyildiz et al.,
75 2017). We chose to examine direct exposure of three key types of cells relevant to environmental
76 exposures and subsequent propagation and transmission of induced epimutations *in vivo* – somatic cell
77 types known to be responsive to endocrine signaling (Sertoli cells and granulosa cells), pluripotent cells
78 (iPSCs) mimicking the preimplantation embryo, and germline cells (PGCLCs).

79 While there have been reports that have clearly indicated the ability of EDCs to disrupt classical
80 endocrine signaling (Henley and Korach, 2010; Kelce et al., 1995; Swedenborg et al., 2009; vom Saal and
81 Hughes, 2005; You et al., 1998), there exist other reports indicating EDCs can also disrupt non-classical
82 endocrine signaling via nuclear receptors (Ozgyin et al., 2015; Song et al., 2011), G protein-coupled
83 receptors (Thomas and Dong, 2006), and calcium channel signaling (Brenker et al., 2018). This has
84 further complicated our understanding of the mechanism(s) by which EDC exposure initially induces
85 epimutations, and has particularly confounded insight into the susceptibility of germ cells to EDC-
86 induced epimutagenesis given that germ cells are reported to lack expression of classical endocrine
87 receptors (Meccariello et al., 2014). This is relevant to the effort to understand mechanisms underlying
88 transgenerational epigenetic inheritance of EDC-induced epimutations (Anway et al., 2006; Guerrero-
89 Bosagna et al., 2012; Nilsson et al., 2008) which clearly implicates transmission via the germ line.

90 The concept of germline transmission of EDC-induced epimutations is further confounded by the
91 known epigenetic reprogramming events that occur in the preimplantation embryo and developing fetal
92 and neonatal germ line. Thus, regardless of how EDC-induced epimutations become initially manifest in
93 the germ line, it is not clear how they subsequently persist and are transmitted inter- or

94 transgenerationally given the large portion of the epigenome that undergoes genome-wide erasure and
95 resetting of epigenetic programming during each generation (Cantone and Fisher, 2013; Lee et al., 2014;
96 Santos et al., 2002; Sanz et al., 2010). *In vitro* cell culture systems afford the opportunity to focus on
97 individual cell types independently, including somatic cells which are likely initially exposed to most
98 environmental disruptive influences, pluripotent cells which represent the preimplantation embryo in
99 which the first major reprogramming event occurs during normal development, and early germline cells
100 where the second major reprogramming event is initiated in primordial germ cells (PGCs). Importantly,
101 in addition to the potential to study each of these cell types independently, it is possible to induce
102 transitions in cell fate *in vitro* that model those that occur during normal development, thereby
103 recapitulating normal reprogramming events in a way that can facilitate high resolution studies of the
104 fate of EDC-induced epimutations once they have been induced in any of these cell types.

105 Here we describe our study of the relative susceptibility to induction of epimutations by direct
106 exposure of four different cell types maintained in culture – somatic Sertoli and granulosa cells,
107 pluripotent iPSCs and germline PGCLCs – to BPS, followed by our analysis of the fate of epimutations
108 initially induced in mouse iPSCs that are then induced to transition into PGCLCs. We found that there are
109 cell type-specific differences in susceptibility to epimutagenesis and associated dysregulation of gene
110 expression patterns following exposure of these different cell types to a similar dose of BPS below the
111 maximum safe exposure limit established for BPA by the EPA (Ribeiro et al., 2019). We further found
112 that these differences correlate at least partially with differential expression of relevant hormone
113 receptors, although germ cells, which do not express relevant receptors, also incurred epimutations
114 following direct exposure to BPS, albeit less extensively than somatic or pluripotent cell types. In all cell
115 types tested, exposure to BPS disrupted epigenetic programming in potentially important regulatory
116 regions including enhancers and promoters. Beyond this, however, we found that the distribution of
117 many of the epimutations induced by exposure to BPS, which is an estrogen mimetic, correlated with

118 the genomic locations of estrogen response elements (EREs) in cell types expressing estrogen receptors,
119 but much less so in germ cells that do not express estrogen receptors. To address the origin of these
120 BPS-induced epimutations in PGCLCs, we identified G-protein coupled receptor targets that potentially
121 could be involved in non-canonical estrogen signaling and susceptibility to BPS exposure. Most
122 interestingly, we found that when iPSCs exposed to BPS were then induced to undergo a major
123 transition in cell fate and related epigenetic reprogramming to form PGCLCs, a similar prevalence of
124 epimutations and DEGs was retained throughout this transition, but very few (<10%) specific
125 epimutations or DEGs were conserved during this process. This suggests that the initial EDC exposure
126 induces a disruption of the chromatin landscape that subsequent epigenetic reprogramming is unable to
127 fully restore. Thus, reprogramming during a major cell fate transition involving cells exposed to BPS
128 appears to correct many of the initially induced epimutations, but also appears to induce many *de novo*
129 epimutations, and this imbalance may persist across multiple generations. This represents a novel
130 mechanism that may underlie continued transgenerational epigenetic inheritance of a prevalence of
131 EDC-induced epimutations despite ongoing generational reprogramming during succeeding generations.

132

133 **Results**

134 **Dose dependent epimutagenesis response to BPS exposure in iPSCs**

135 To initially assess the extent to which epimutations and dysregulated gene expression can be
136 induced in cells maintained in culture, we exposed mouse iPSCs to three doses of BPS (1, 50, and 100
137 μM) and measured the impact on the epigenome and transcriptome using the Illumina Infinium Mouse
138 Methylation BeadChip Array and RNA-seq, respectively (Figure 1). All three doses of BPS induced
139 individual differentially methylated CpGs (DMCs) as well as differentially methylated regions (DMRs)
140 (Figure 1a), and differentially expressed genes (DEGs) (Figure 1b) when compared to control mouse

141 iPSCs treated with vehicle (EtOH) only. The extent of this exposure-specific epimutagenesis was directly
142 correlated with the dose of BPS used. These results provided an initial proof of concept that exposure of
143 cells maintained *in vitro* to an EDC such as BPS can disrupt the epigenome and transcriptome in a dose-
144 dependent manner. Interestingly, exposure to 1 µM BPS induced very few DMRs, but did induce
145 widespread DMCs and DEGs. Because 1 µM BPS is below the FDA's suggested safe environmental level
146 established for BPA (Ribeiro et al., 2019), and was sufficient to induce DMCs and dysregulated gene
147 expression on all chromosomes, we utilized this dose and focused solely on DMCs when assessing
148 epimutations in all subsequent experiments.

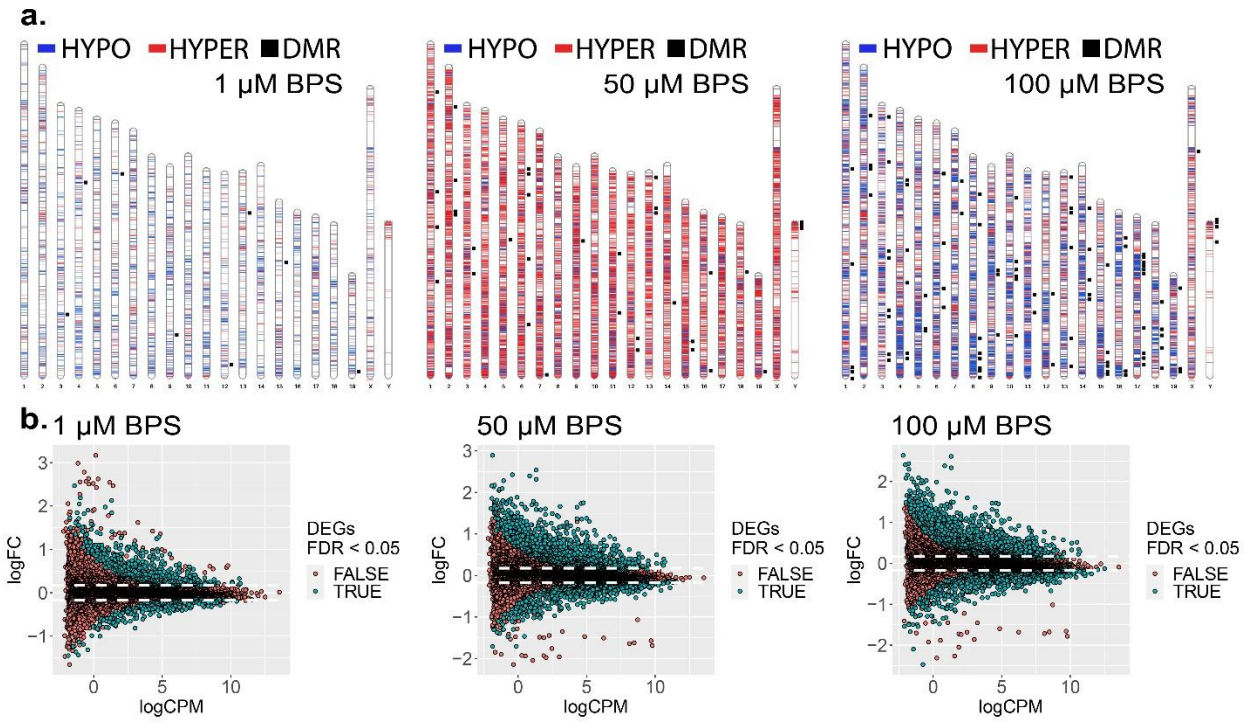

149

150 **Figure 1. Dose dependent impact of epimutagenesis measured in iPSCs exposed to 1, 50, and 100 µM**
151 **BPS. a)** Ideogram plots displaying chromosomal distribution of genome-wide changes in DNA
152 methylation caused by BPS exposure. **b)** Mean difference (MD) plots of changes in gene expression
153 following exposure to increasing doses of BPS. Exposure to increasing doses of BPS induced
154 corresponding increases in the numbers of DMCs, DMRs, and DEGs. Blue horizontal lines =
155 hypomethylated DMCs, red horizontal lines = hypermethylated DMCs, black squares = DMRs.

156

157

Cell type-specific susceptibility to induction of epimutations following BPS exposure

We next sought to determine if different key cell types – somatic, pluripotent and germ – are differentially susceptible to induction of epimutations in response to direct exposure of each to a similar dose of BPS. Thus, we exposed pluripotent (iPSCs), somatic (Sertoli and granulosa cells), and germ (PGCLCs) cell types to 1 µM BPS and measured changes in DNA methylation patterns. We identified exposure-specific DMCs in each exposed cell type relative to its corresponding control (exposed to carrier only) (Figure 2a). We observed overall differences among the different cell types in total numbers of DMCs, with iPSCs showing the highest number of DMCs, followed by Sertoli cells and granulosa cells, and then PGCLCs, respectively (Table 1).

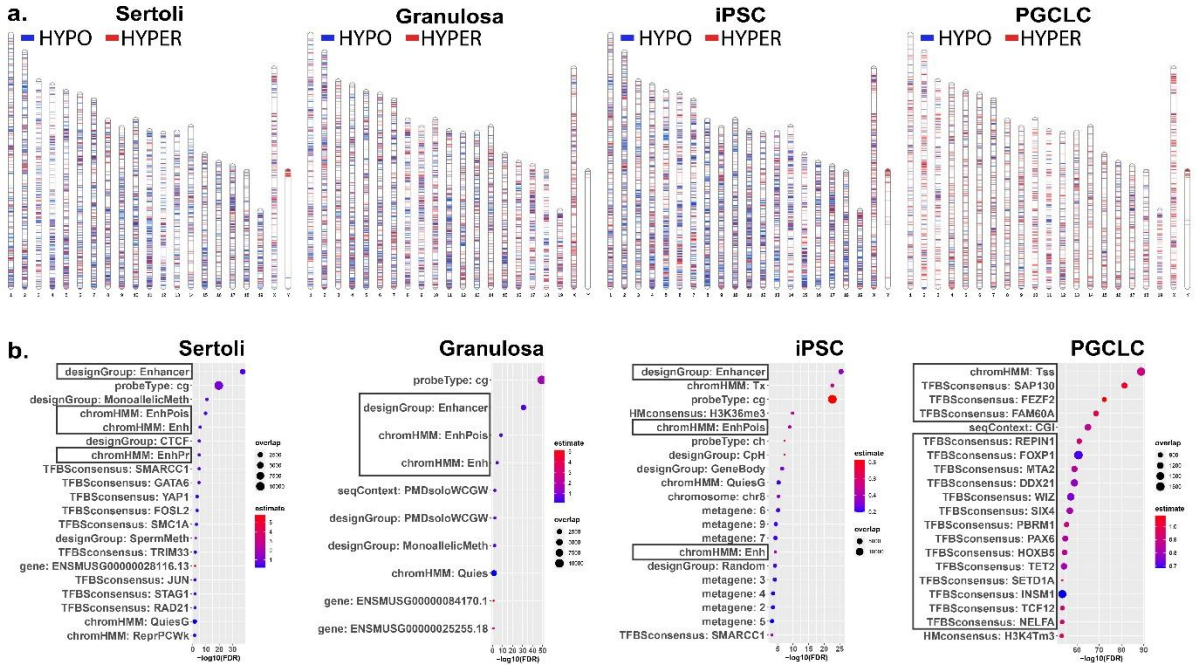

Figure 2. Chromosomal distributions and annotations of BPS-induced epimutations in pluripotent, somatic, and germ cell types. a) Ideograms illustrating chromosomal locations of DMCs induced by exposure of each cell type to 1 µM BPS. Blue horizontal lines = hypomethylated DMCs, red horizontal lines = hypermethylated DMCs. **b)** Enrichment plots indicating feature annotations in genomic regions displaying prevalent BPS-induced epimutations in each cell type.

Table 1. Treatment-specific differentially methylated sites (DMCs) (treated vs. control)				
DMCs	**Sertoli**	**Granulosa**	**iPSCs**	**PGCLCs**
Hypomethylated[1]	7,385	6,444	9,651	2,315
Hypermethylated[2]	3,022	4,143	4,308	4,785
Total	10,407	10,587	13,959	7,100

174 [1]A CpG site that was predominantly methylated in the control samples but unmethylated in the exposed
175 samples.
176 [2]A CpG site that was predominantly unmethylated in the control samples but methylated in the exposed
177 samples.

178

179 Interestingly, among the exposure-specific DMCs identified in each cell type, we observed
180 predominantly hypomethylated DMCs in the somatic and pluripotent cell types, but predominantly
181 hypermethylated DMCs in PGCLCs (Table 1). These findings confirm that there are both quantitative
182 differences among cell types in overall susceptibility to epimutagenesis, and qualitative cell type-specific
183 differences in the prevalence of hypo- versus hypermethylated DMCs following exposure to BPS. The
184 latter likely reflects the fact that the epigenome in PGCs is naturally more hypomethylated than that in
185 pluripotent or somatic cell types (Hajkova, 2011), enhancing the likelihood that most changes in DNA
186 methylation induced in PGCLCs will necessarily involve hypermethylation.

187 **Annotation of BPS-induced epimutations**

188 We next analyzed annotations associated with genomic sites of BPS exposure-specific DMCs in
189 each cell type. We mined annotations associated with genomic regions included on the Infinium array
190 and found that a substantial group of exposure-specific DMCs was associated with enhancer regions in
191 the two somatic (Sertoli and granulosa) and one pluripotent (iPS) cell types exposed to BPS, while in
192 PGCLCs BPS-induced DMCs were more prevalent at promoter regions containing transcription start sites

193 (TSSs) and transcription factor binding sites (Figure 2b), indicative of yet another qualitative cell type-
194 specific difference in induction of epimutations by the same dose of BPS.

195

196 **Relationship between susceptibility to BPS-induced epimutagenesis and expression of relevant**
197 **hormone receptors**

198 As EDCs are thought to induce epimutations via disruption of classical hormonal signaling
199 (Henley and Korach, 2010; Kelce et al., 1995; Swedenborg et al., 2009; vom Saal and Hughes, 2005; You
200 et al., 1998), we next sought to determine if the differential extent of BPS induction of epimutations we
201 observed in different cell types was associated with differential expression of relevant hormone
202 receptors in each. We performed immunocytochemistry (ICC) to detect the presence of the relevant
203 estrogen receptors – ERα and ERβ, while co-staining for cell type-specific markers (WT1 [Sertoli cell
204 marker], FSHR [granulosa cell marker], FUT4 [iPSC marker], and NANOG [PGCLC or endogenous PGC
205 marker]) to confirm the identity of the four cultured cell types examined in this study (Sertoli cells,
206 granulosa cells, iPSCs and PGCLCs), as well as endogenous mouse PGCs (Figure 3a). Both somatic cell
207 types (Sertoli and granulosa) showed positive immunolabeling for both ERα and ERβ, whereas the
208 pluripotent cells showed positive immunolabeling for ERβ, but negative immunolabeling for ERα, and
209 the PGCLCs and endogenous PGCs showed negative immunolabeling for both ERα and ERβ. Importantly,
210 the latter result is consistent with previous reports of lack of expression of either ERα or ERβ at the
211 protein level in endogenous PGCs (Meccariello et al., 2014).

212 These results demonstrate cell type-specific differences in expression of hormone receptors
213 (ERα and ERβ) which are potentially relevant to the disruptive action of the estrogen mimetic, BPS. We
214 noted that expression of at least one potentially relevant hormone receptor (ERβ) in either somatic or
215 pluripotent cells correlated with a higher incidence of DMCs induced by exposure of somatic or

216 pluripotent cell types to 1 µM BPS relative to the incidence of DMCs induced by exposure of PGCLCs,
217 which do not express either estrogen receptor, to the same dose of BPS (Table 1). Nevertheless, we did
218 still observe induction of DMCs when PGCLCs were exposed to BPS, demonstrating that expression of
219 relevant canonical hormone receptors is not an absolute requirement for induction of epimutations in
220 response to an EDC. As noted above, we also observed differences in annotations of the genomic
221 regions in which BPS induced epimutations in germ cells relative to the other cell types tested, with ERα-
222 and/or ERβ-expressing somatic and pluripotent cell types showing a higher incidence of epimutations at
223 apparent enhancer regions while ERα-/ERβ-negative germ cells showed a higher epimutation incidence
224 at apparent promoter regions (900 bp upstream and 500 bp downstream from TSS) (Figure 2b). Taken
225 together, these results reveal cell type-specific differences in susceptibility to induction of epimutations
226 by exposure to the EDC, BPS.

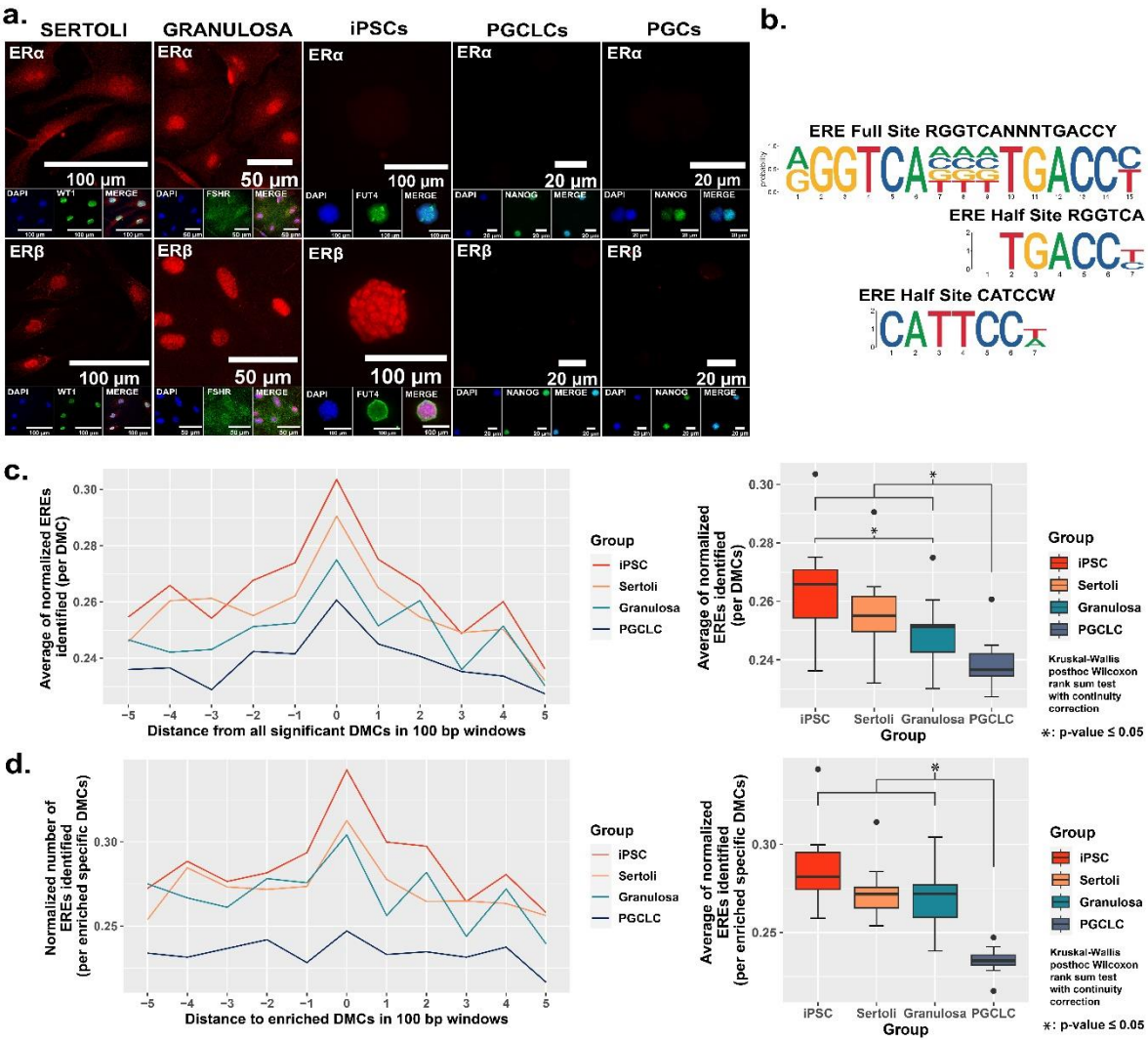

Figure 3. Correlation between cell type-specific expression of estrogen receptors and density of genomic EREs associated with BPS-induced epimutations. a) Assessment of expression of ERα and ERβ on cell types co-stained for known cell type-specific markers. Somatic cell types express both receptors, pluripotent cells express ERβ but not ERα, and germ cells do not express either estrogen receptor. **b)** Motif plots displaying the full ERE consensus sequence and the more biologically relevant ERE half-site motifs found to be enriched from ERα ChIP-seq. **c,d)** Normalized density plots and box plots displaying the frequency of ERE half-sites identified c) within 500 bp of all BPS-induced DMCs genome-wide, or d) within 500 bp of the most enriched categories of BPS-induced DMCs in each cell type (= enhancer regions for somatic and pluripotent cell types and promoter regions in the germ cell type).

Proximity of BPS-induced epimutations to genomic EREs

240 The relatively higher incidence of BPS-induced epimutations in cell types expressing one or both
241 estrogen receptor(s) suggests BPS-induced epimutagenesis may be manifest, at least in part, through
242 canonical endocrine signaling pathways. If this is the case, we might expect to see elevated induction of
243 epimutations in genomic regions enriched for relevant HREs which, for interactions with the estrogen
244 mimetic, BPS, would be EREs. Previous studies have defined a full ERE consensus sequence (Bourdeau et
245 al., 2004), but other reports have indicated that estrogen receptors can often bind to ERE half-sites
246 (Mason et al., 2010) (Figure 3b). Indeed, when we mined publicly available ERα ChIP-seq peaks from the
247 UCSC genome browser database (Dunham et al., 2012; Myers et al., 2011; Sloan et al., 2016; Wang et
248 al., 2013, 2012) and performed motif enrichment, we identified two distinct ERE half-sites within regions
249 enriched for DMCs rather than one full sized ERE consensus sequence, with the half-sites appearing to
250 be more biologically relevant to interaction with estrogen or its mimetics (Figure 3b). We then plotted
251 the frequency of ERE half-sites in genomic regions within 500 bp of BPS-induced epimutations (Figure
252 3c,d). We found an increase in the frequency of ERE half-sites identified within 500 bp of BPS-induced
253 DMCs genome-wide in all four cell types investigated, although the frequency was notably lower in germ
254 cells (Figure 3c). Interestingly, this higher frequency of ERE half-sites within 500 bp of BPS-induced DMCs
255 was conserved in three of the four cell types – somatic (Sertoli and granulosa) and pluripotent (iPSCs)
256 when we focused solely on apparent enhancer regions, but not in germ cells (PGCLCs) where the
257 majority of DMCs occurred at apparent promoter regions (Figure 3d). We also mined the UCSC mouse
258 genome sequence for genome-wide prevalence of ERE half-sites and found that while these sites occur
259 in both promoter and enhancer regions, they are nearly four-fold more frequent in enhancers
260 (Supplementary file 1b). Thus, it is perhaps not surprising that BPS-induced epimutations were more
261 prevalent in enhancer regions in somatic and pluripotent cell types that express one or both ERs, than in
262 germ cells that do not express either ER.

263 Taken together, these results suggest a relationship between i) expression of either ERβ alone or
264 ERα and ERβ together, ii) elevated susceptibility to BPS-induced epimutagenesis, and iii) the occurrence
265 of BPS-induced DMCs in genomic regions – particularly enhancers – containing EREs. These observations
266 are consistent with the notion that one mechanism contributing to EDC-based induction of epimutations
267 involves disruption of canonical endocrine signaling pathways. However, the fact that exposure to BPS
268 also induced epimutations in germ cells, even in the absence of expression of estrogen-related
269 receptors, and generated many DMCs in regions not inclusive of EREs, suggests that disruption of
270 canonical endocrine signaling pathways is not the only mechanism by which exposure to an EDC can
271 induce epimutations.

272 **Cell type-specific features of BPS-induced epimutations**

273 To further interrogate cell type-specific differences in the genesis of epimutations following
274 exposure to BPS, we compared DNA methylation patterns detected in the control (vehicle only) samples
275 to identify naturally occurring, cell type-specific DMCs inherently associated with each different cell fate.
276 Interestingly, of the 297,415 distinct CpGs interrogated by the Illumina Infinium Mouse Methylation
277 BeadChip Array used for this analysis, >240,000 showed some degree of inherent differential
278 methylation among the four cell types tested, suggesting they are tied to cell-fate specific differential
279 DNA methylation (Figure 4a). We next determined the extent to which DMCs induced specifically by
280 exposure of each cell type to BPS occurred at CpG dinucleotides that were among these naturally
281 occurring cell type-specific DMCs. We found that a large majority of BPS exposure-specific epimutations
282 detected in each cell type occurred at CpGs that also show inherent, cell type-specific variation in DNA
283 methylation (>95% of BPS-induced epimutations in somatic and pluripotent cell types and ~89% in germ
284 cells) (Figure 4a). As with the overall pattern of BPS-induced epimutations shown in Figure 2, BPS-
285 induced epimutations at CpGs showing inherent cell type-specific variation were enriched in apparent
286 enhancer regions that occurred near EREs in somatic and pluripotent cell types, whereas those in germ

287 cells were found predominantly in promoter regions containing significantly fewer EREs (Figure 4b,d).
288 However, the low percentage of BPS-induced epimutations that occurred at CpGs that did not show
289 inherent cell type-specific variation in DNA methylation patterns were found to be enriched in promoter
290 regions lacking nearby EREs in all four cell types (Figure 4c,d). Thus, this latter group of BPS-induced
291 epimutations appears to represent a small core group that arises following exposure to BPS via a
292 mechanism that does not rely upon disruption of canonical endocrine signaling, and so is common to all
293 cell types, regardless of expression of relevant endocrine receptors or nearby residence of relevant HREs
294 within the genome.

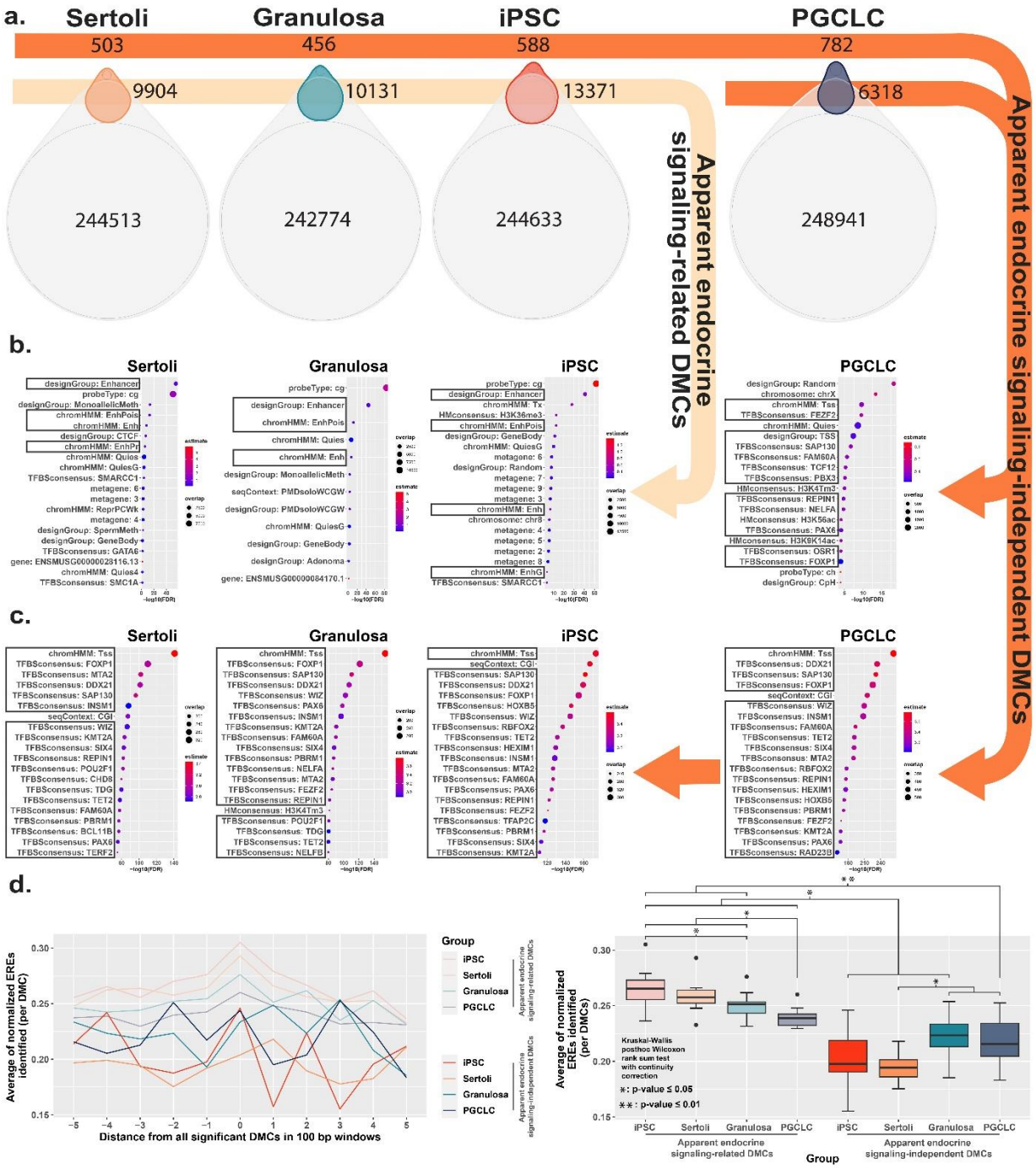

295

296 **Figure 4. Direct comparison of BPS exposure-specific and cell type-specific features between cell**
297 **types. a)** Assessment Venn diagrams indicating DMCs that are due either to BPS exposure (top, smaller
298 ovals) or inherent cell type-specific differences (bottom, larger ovals). Numbers of apparent endocrine
299 signaling-related DMCs are shown in the light orange arrow, and apparent endocrine signaling-
300 independent DMCs are shown in the dark orange arrows. Enrichment plots indicating feature
301 annotations in genomic regions displaying **b)** apparent endocrine signaling-related DMCs occurring
302 predominantly in enhancer regions in somatic Sertoli and granulosa cell types or pluripotent cells

303 expressing one or more estrogen receptors, or **c)** a smaller set of apparent endocrine signaling-
304 independent DMCs occurring predominantly in promoter regions in all four cell types regardless of +/-
305 expression of relevant endocrine receptors. **d)** Normalized density plots and box plots displaying the
306 frequency of ERE half-sites identified within 500 bp of apparent endocrine signaling-related DMCs
307 occurring predominantly in enhancer regions and apparent endocrine signaling-independent DMCs
308 occurring predominantly in promoters.

309

310 **Impact of BPS exposure on gene expression**

311 We next sought to determine if the cell type-specific differential susceptibility to BPS-induced
312 epimutagenesis translated to a similar extent of dysregulation of gene expression in each cell type.
313 Somewhat surprisingly, RNA-seq analysis of gene expression patterns in each exposed cell type relative
314 to its corresponding control (same cell type exposed to carrier only) revealed the greatest number of
315 dysregulated genes in PGCLCs, despite PGCLCs being the cell type that showed the lowest number of
316 epimutations following exposure to BPS (Tables 1,2). iPSCs showed the second highest level of
317 dysregulated genes, while somatic Sertoli and granulosa cells showed very low levels of dysregulated
318 gene expression (Table 2). Indeed, numbers of dysregulated genes were three orders of magnitude
319 lower in differentiated somatic cells than in either pluripotent cells or germ cells (Table 2).

320 Because BPS-exposed PGCLCs showed the highest level of dysregulated genes, as well as the
321 highest enrichment of DMCs occurring primarily at promoters (Figure 2b), we next assessed the general
322 proximity between DMCs and promoter regions in each cell type to determine if DMCs in promoter
323 regions may be more likely to predispose dysregulated gene expression than DMCs elsewhere in the
324 genome (Figure 5a). Indeed, we found that in all four cell types, the smaller the median distance
325 between BPS-induced DMCs and neighboring promoter regions, the larger the number of BPS-induced
326 DEGs (Figure 5b). Thus, it appears that while PGCLCs showed the fewest BPS-induced DMCs among the
327 four cell types exposed to BPS, this exposure induced a higher proportion of epimutations in regions
328 within or adjacent to promoters in this cell type. This, and the relatively high extent of decondensed

329 chromatin genome-wide in fetal germ cells, appear to have contributed to the higher incidence of
330 dysregulated gene expression in BPS-exposed PGCLCs than that observed in the other three BPS-
331 exposed cell types, even though the overall numbers of BPS-induced epimutations were greater in the
332 other cell types.

333

Table 2. Exposure-specific differentially expressed genes*

DEGs	Sertoli	Granulosa	iPSCs	PGCLCs
Down regulated	3	0	343	844
Up regulated	32	2	694	1,046
Total	35	2	1,037	1,890

334 *Genes showing significant differential expression following exposure of each cell type to 1µM BPS
335 relative to matched control cell types exposed to carrier only.

336

337

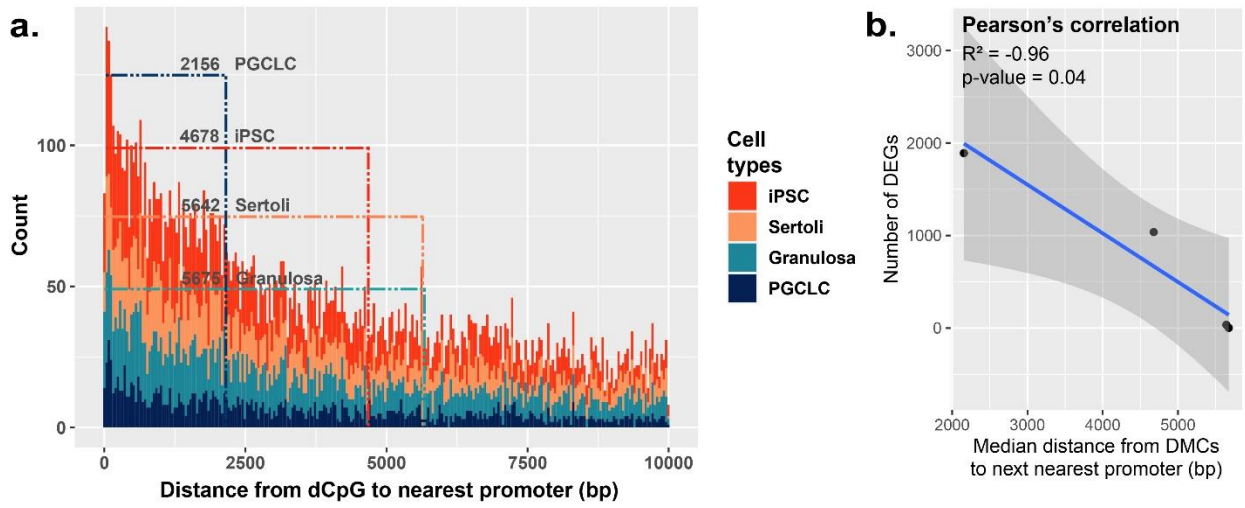

338

339 **Figure 5. Correlation between the proximity of DMCs to promoters and dysregulation of gene**
340 **expression. a)** Proximity plot displaying distances from exposure-specific DMCs to nearest promoter

341 regions. Dotted lines indicate median points of the data for each cell type. **b)** Correlation plot displaying
342 a negative relationship between the distance from DMCs to nearest promoters and resulting
343 dysregulation of gene expression within each cell type.

344

345 **Potential non-canonical signaling pathways disrupted by BPS exposure**

346 To identify potential mechanisms by which BPS exposure may induce epimutations via
347 disruption of non-canonical endocrine signaling pathways, we mined our RNA-seq data to identify genes
348 dysregulated independently of expression of relevant hormone receptors or presence of nearby EREs.
349 We identified a set of genes in all four cell types tested that displayed promoters enriched for apparent
350 endocrine-signaling independent DMCs (Supplementary file 1a). Gene ontology (GO) analysis indicated
351 that several of the 1,957 genes we identified were associated with ubiquitin-like protease pathways,
352 including 124 of 800 genes that regulate protein degradation and 5 of 9 genes involving 1-
353 phosphatidylinositol-3 kinase activities, linked to the PI3K/AKT signaling pathway (Figure 6a). Previous
354 reports have established a link between ubiquitin-like protease pathways and classical ER signaling
355 (Beamish and Frick, 2022; Kabir et al., 2015), suggesting that genes with promoters lacking EREs may be
356 regulated by factors encoded by genes with promoters containing EREs, and so could be indirectly
357 activated or repressed by disruption of classical ER signaling. Further, involvement of PI3K/AKT pathway
358 signaling has previously been linked to estrogen signaling through G-protein coupled receptors such as
359 GPER1, which was implicated in non-canonical estrogen signaling in ER KO mouse cell lines (Filardo et
360 al., 2002; Molina et al., 2017). To determine if our data support this suggestion, we performed GO
361 analysis on the 1,890 DEGs identified in PGCLCs in which epimutations appeared to be induced
362 independent of classical ER signaling. We detected no apparent involvement of pathways involving
363 ubiquitin-like proteases, but we did detect differential expression of 4 of 7 genes associated with a
364 pathway involving phosphatidylinositol-4 phosphatase signaling which intersects with the PI3K/AKT
365 signaling pathway (Figure 6b). Finally, while we did not detect differential expression of *Gper1*

transcripts, we did observe differential expression of genes encoding other less well studied G-protein coupled receptors, including *Gprc5a*, *Gprc5b*, *Gpr89, Gpr107*, and *Gpr161* in all four cell types exposed to BPS. These receptors have all been previously shown to bind either BPA or 17β-estradiol in rat models (https://rgd.mcw.edu/rgdweb/report/gene/main.html?id=1305882, https://rgd.mcw.edu/rgdweb/report/gene/main.html?id=1563245, https://rgd.mcw.edu/rgdweb/report/gene/main.html?id=1304837, https://rgd.mcw.edu/rgdweb/report/gene/main.html?id=1310804, https://rgd.mcw.edu/rgdweb/report/gene/main.html?id=1309510) and could be potential targets of non-canonical BPS-induced estrogen signaling (Figure 6c).

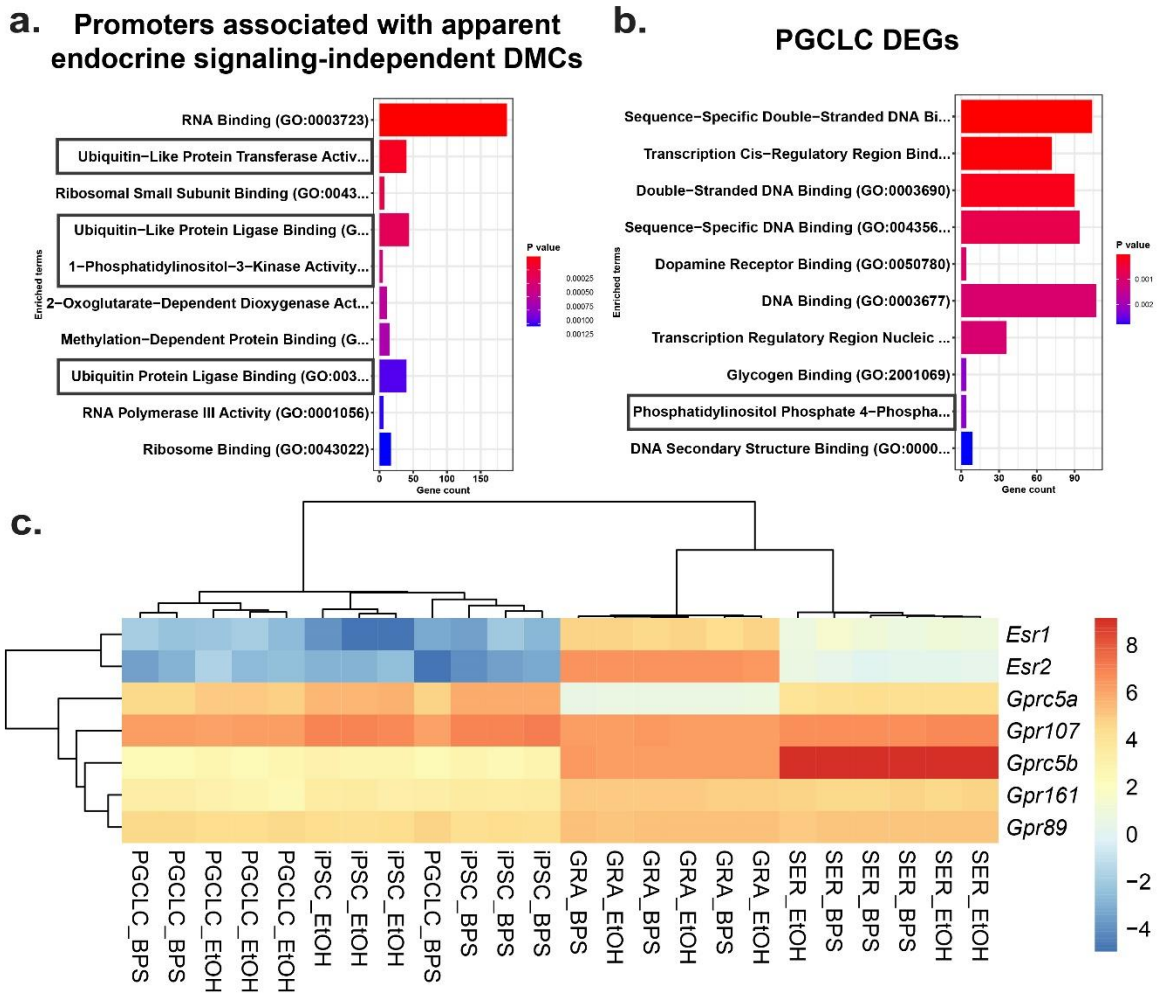

375

376 **Figure 6. Potential involvement of non-canonical estrogen signaling pathways in BPS-induction of**
377 **epimutations.** Relative expression of genes **a)** enriched for apparent endocrine signaling-independent
378 promoter-region DMCs or **b)** dysregulated in PGCLCs which lack expression of estrogen receptors. **c)**
379 Heatmap of relative expression of estrogen receptor genes (*Esr1* and *Esr2*) and G-coupled protein
380 receptors (*Gprc5a*, *Gpr107*, *Gprc5b*, *Gpr161*, and *Gpr89*) in pluripotent, somatic, and germ cell types.

381

382 **Propagation of BPS-induced epimutations during transitions in cell fate**

383 Transitions between pluripotent and germ cell fates, or vice versa, are accompanied by large-
384 scale epigenetic reprogramming *in vivo* (Cantone and Fisher, 2013; Lee et al., 2014; Santos et al., 2002;
385 Sanz et al., 2010), and these are recapitulated during similar transitions induced *in vitro* (Ishikura et al.,
386 2016). To determine the extent to which BPS-induced epimutations persist during a pluripotent to
387 germline transition *in vitro*, we first exposed iPSCs to 1 µM BPS and then differentiated the exposed
388 iPSCs first into epiblast-like cells (EpiLCs) and then into PGCLCs recapitulating the early germline
389 epigenetic reprogramming event that normally occurs *in vivo* (Kurimoto and Saitou, 2018; Ohta et al.,
390 2017) (Figure 7a). We then compared the numbers of exposure-specific DMCs and DEGs detected in the
391 PGCLCs derived from the BPS-exposed iPSCs with those in the directly exposed iPSCs and found lower,
392 but still substantial numbers of both (28,168 vs 38,105 DMCs, and 1,437 vs 1,637 DEGs in the derived
393 PGCLCs and directly exposed iPSCs, respectively) (Figure 7b,c). However, when we compared the <u>specific</u>
394 DMCs and DEGs that were detected in the BPS-exposed iPSCs with those that were detected in the
395 subsequently derived PGCLCs, we found that >90% of each were not conserved during the pluripotent to
396 germline transition in cell fate. Specifically, only 3.7% of the DMCs and 8.4% of the DEGs detected in the
397 BPS-exposed iPSCs were also detected in the PGCLCs derived from the exposed iPSCs. Thus, of the
398 38,105 DMCs and 1,637 DEGs induced by exposure of iPSCs to 1 µM BPS, 36,688 and 1,499, respectively,
399 did not persist during differentiation of the iPSCs to form PGCLCs and so were apparently corrected by
400 germline reprogramming. Simultaneously however, 26,752 novel DMCs and 1,299 novel DEGs appeared
401 in the PGCLCs that were not present in the BPS-exposed iPSCs, so were apparently generated *de novo*

during the germline reprogramming process. These results are consistent with the notion that germline epigenetic reprogramming corrected many of the epimutations that were present in the BPS-exposed pluripotent cells from which they were derived, but that exposure of cells to EDCs may disrupt the underlying chromatin landscape in a way that then interferes with subsequent reprogramming such that in addition to correcting many previously induced epimutations, the germline reprogramming process, acting on a disrupted chromatin landscape, also generates many novel epimutations *de novo* during the pluripotent to germline transition.

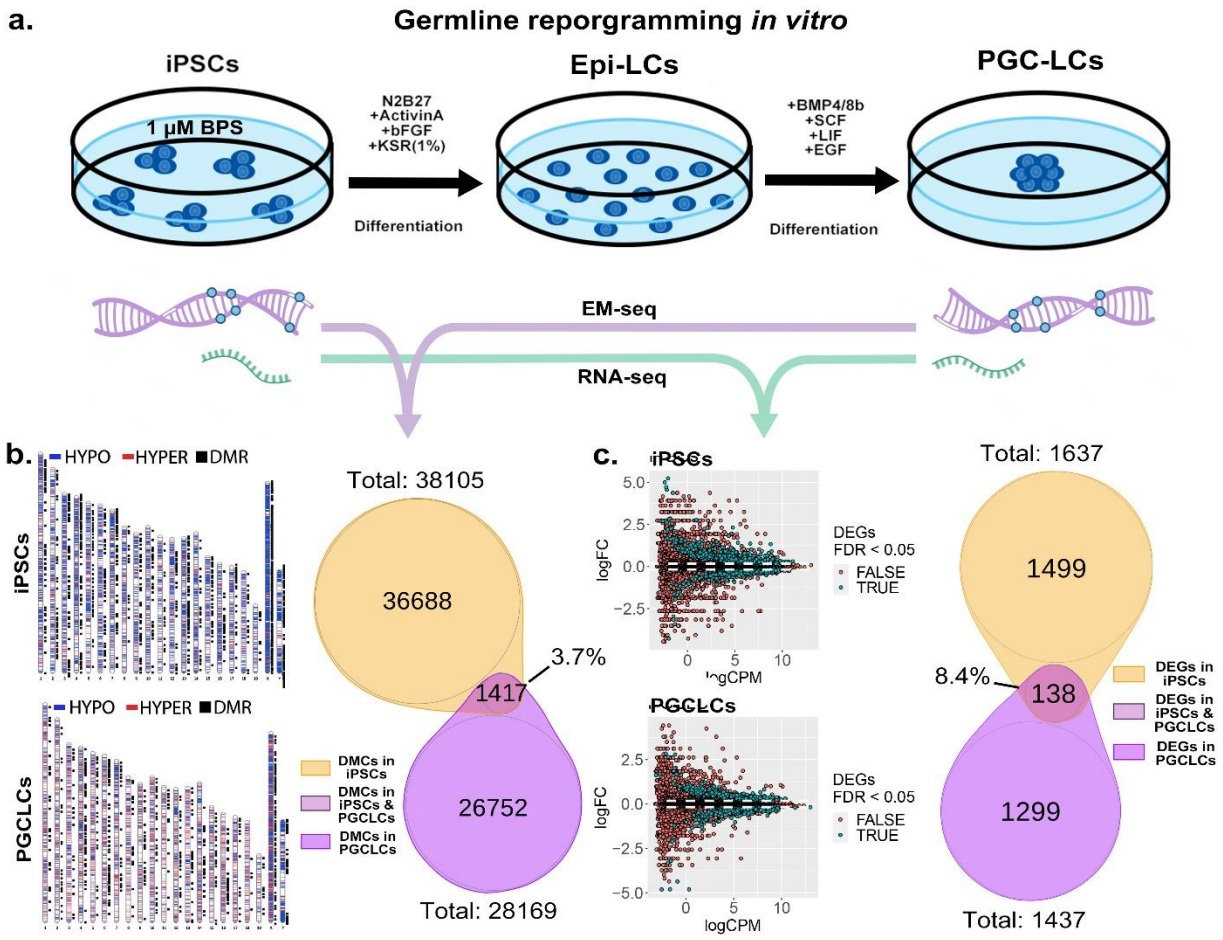

Figure 7. Persistence of BPS-induced epimutations through recapitulation of early germline reprogramming *in vitro*. a) Schematic illustrating derivation of PGCLCs from iPSCs *in vitro*. iPSCs are first induced to form EpiLCs which are then induced to form PGCLCs. iPSCs were exposed to either ethanol + 1 µM BPS or ethanol (carrier) only, then induced to undergo transitions to form EpiLCs and then PGCLCs. **b)** DNA samples from BPS-exposed or control iPSCs as well as subsequently derived PGCLCs were assessed for DNA methylation epimutations by EM-seq. BPS-treated iPSCs showed 38,105 DMCs and

416 subsequently derived PGCLCs showed 28,169 DMCs. Of those, only 1,417 (3.7%) of the DMCs were
417 conserved from the BPS-exposed iPSCs to the subsequently derived PGCLCs. **c)** RNA samples from BPS-
418 exposed or control iPSCs and subsequently derived PGCLCs were assessed for global gene expression
419 patterns by RNA-seq. BPS-treated iPSCs showed 1,637 exposure-specific DEGs and subsequently derived
420 PGCLCs showed 1,437 exposure-specific DEGs. Of those, only 138 (8.4%) were conserved from the BPS-
421 exposed iPSCs to the subsequently derived PGCLCs.

422

423 **Discussion**

424 While nearly 20 years of research on the effects of exposure of live animals to various EDCs and
425 other environmental disruptive influences has clearly established the potential to perturb the
426 epigenome in ways that can dysregulate normal gene expression patterns and predispose the
427 development of disease states, the molecular mechanisms underlying these phenomena have remained
428 largely undefined. Thus, the manner in which environmental exposures introduce biochemical changes
429 in epigenetic programming, how such disruptions can be propagated within a tissue or throughout the
430 soma of an exposed individual or enter that individual's germ line, or how these disruptions predispose
431 disease states in that individual, or how a resulting prevalence of epimutations can be transmitted to
432 multiple subsequent generations despite generational epigenetic reprogramming, are all mechanistic
433 questions that have remained unanswered despite more than 5,000 publications on this topic since the
434 early 2000s. The vast majority of those publications have described experiments in animal models –
435 typically rodents. While informative, such live animal studies require months to years to complete, are
436 cost- and animal-intensive, and have not yielded insight into the molecular mechanisms underlying the
437 deleterious effects of environmentally-induced epimutations.

438 *In vitro* model systems have proven to be very useful tools for deciphering molecular
439 mechanisms related to normal development and homeostasis, or disruptions of those processes
440 predisposing onset of disease. Examples include cell culture systems used to study developmental
441 processes such as X-chromosome inactivation in mammals (Almeida et al., 2017; Patrat et al., 2009) or

442 early embryogenesis (Bao et al., 2022; Lau et al., 2022), or to elucidate the cellular and molecular
443 etiology of many different diseases based on the now popular "disease-in-a-dish" approach (Davaapil et
444 al., 2020; Song et al., 2023). We assembled an *in vitro* system in which we combined the three cell types
445 normally involved in i) the initial exposure to disruptive environmental effects (somatic cells), ii) the first
446 phase of generational epigenetic reprogramming in the preimplantation embryo (pluripotent cells), and
447 iii) the second phase of generational reprogramming in the developing germ line (germ cells). This
448 system allowed us to gain insights into multiple mechanistic aspects of environmentally-induced
449 epimutagenesis including the initial induction of epimutations by exposure of cells to the EDC, BPS, cell
450 type-specific differences in susceptibility to BPS-induced epimutagenesis, factors that appear to
451 contribute to that differential susceptibility, and the mechanism by which an epimutated state is
452 transmitted across multiple generations despite generational reprogramming.

453 Here we have shown that exposure of homogeneous populations of cells maintained in culture
454 to an EDC such as BPS can induce epimutagenesis and dysregulation of gene expression, and that this
455 occurs in a dose-dependent manner. This afforded us the opportunity to test the relative effects of
456 direct exposure of different specific cell types to a similar dose of BPS with no confounding effects
457 imposed by interactions with other cell types or systemic effects of the sort that normally occur in the *in*
458 *vivo* context. We found that somatic, pluripotent and germ cell types do indeed show differences in
459 direct susceptibility to induction of epimutations following exposure to BPS, both in terms of the
460 quantity of epimutations induced and qualities of the resulting epimutations such as a predominance of
461 hyper- versus hypomethylation, and the genomic locations where such epimutations tend to occur. Our
462 results suggest that these differences reflect distinctions in the normal status of each cell type at the
463 time of exposure. Thus, somatic, pluripotent and germ cell types differ in the normal status of genome-
464 wide patterns of accessible versus inaccessible chromatin, global DNA methylation, and expression of
465 relevant endocrine receptors. Interestingly, our data suggest that all of these parameters can influence

466 cell type-specific susceptibility to induction of epimutations by exposure to BPS, and that different
467 combinations of these variables ultimately determine the quantity and quality of epimutations induced
468 by exposure to BPS.

469 Endogenous fetal germline cells (e.g. PGCs and prospermatogonia in males) normally display
470 lower levels of global DNA methylation and higher levels of chromatin accessibility than pluripotent or
471 somatic cell types (Hajkova, 2011), yet PGCLCs developed fewer epimutations following exposure to BPS
472 than the other cell types. This appears to be explained by the fact that germline cells do not express
473 either estrogen receptor whereas pluripotent and somatic cell types express one or both of the two
474 estrogen receptors, apparently rendering them more susceptible to induction of epimutations following
475 exposure to the estrogen mimetic, BPS. This is consistent with the notion that EDCs impose disruptive
476 effects by interfering with canonical endocrine signaling pathways, and that notion is further supported
477 by our observation that, in the cell types that express one or both estrogen receptors, we observed a
478 prevalence of BPS-induced epimutations in genomic regions containing nearby EREs, whereas in PGCLCs,
479 which do not express either estrogen receptor, we did not observe a correlation between the locations
480 of BPS-induced epimutations and genomic EREs.

481 Nevertheless, we did observe induction of epimutations in PGCLCs exposed to BPS, suggesting
482 that while cell types expressing relevant endocrine receptors may display elevated susceptibility to EDC-
483 induced epimutagenesis presumably based on disruption of canonical endocrine signaling, this is not the
484 only mechanism by which EDCs can induce epimutations. Indeed, our results support the suggestion
485 that there may be at least two types of epimutations induced by exposure to EDCs – one that is
486 independent of canonical endocrine signaling and so occurs in all cell types regardless of expression of
487 relevant endocrine receptors or the genomic location of relevant HREs, and another that does involve
488 disruption of canonical endocrine signaling and so is elevated in cell types expressing relevant endocrine
489 receptors and predisposes the induction of epimutations in genomic regions near relevant HREs. Beyond

490 this, a comparison of the quantities of BPS-induced epimutations in pluripotent and somatic cell types,
491 which both express one or both estrogen receptors, but which differ with respect to elevated genome-
492 wide chromatin accessibility in pluripotent cells compared to much more limited chromatin accessibility
493 in somatic cell types (Cantone and Fisher, 2013; Santos et al., 2002), suggests that chromatin
494 accessibility also contributes to susceptibility to EDC-induced epimutagenesis.

495 One of our most intriguing findings was that, in addition to estrogen-receptor expressing
496 somatic and pluripotent cell types developing more epimutations than non-estrogen-receptor
497 expressing germ cells in response to exposure to BPS, the occurrence of epimutations in the former
498 (somatic and pluripotent) cell types was predominantly in enhancer regions whereas that in the latter
499 (germ) cell type was predominantly in gene promoters. As noted above, there was a significant increase
500 in the occurrence of BPS-induced epimutations near EREs in somatic and pluripotent cell types
501 compared to germ cells. A genome wide analysis confirmed that ERE half-sites occur more frequently in
502 enhancer regions than in promoter regions (Supplementary file 1b) supporting our suggestion that the
503 higher prevalence of BPS-induced epimutations we observed in enhancer regions in somatic and
504 pluripotent cell types was due to disruption of canonical hormone signaling.

505 Our finding that PGCLCs, which do not express endocrine receptors, still accrued epimutations
506 following exposure to BPS indicates that in addition to inducing epimutations by disrupting canonical
507 endocrine signaling pathways, exposure to EDCs can induce epimutations via mechanisms that do not
508 involve disruption of such pathways. This notion is further supported by the occurrence of BPS-induced
509 epimutations in genomic regions that do not include nearby EREs, even though a prevalence of the
510 epimutations induced in PGCLCs were located in gene promoters. Pathway analysis of the genes in
511 which promoter-region epimutations were induced by exposure of PGCLCs to BPS suggests an apparent
512 endocrine-signaling independent group of genes that can become disrupted by exposure to an EDC via
513 non-canonical signaling which may occur through the PI3K/AKT pathway via G-protein coupled

514 receptors. While we observed expression of a number of G-protein coupled receptors known to bind to
515 either 17β-estradiol or BPA, further studies will be required to determine if any of these contribute to
516 susceptibility to BPS epimutagenesis.

517 As expected, disruption of normal epigenetic programming induced by exposure of cells to BPS
518 also led to dysregulation of gene expression. Thus, RNA-seq analysis detected differentially expressed
519 genes in all cell types exposed to BPS. Surprisingly, the greatest number of DEGs was detected in PGCLCs
520 which was the cell type that developed the lowest overall number of epimutations in response to
521 exposure to BPS. However, PGCLCs showed a higher prevalence of BPS-induced epimutations in gene
522 promoter regions than was observed in any of the other cell types, so it appears that promoter-region
523 epimutations impose the most direct impact on gene expression. As noted above, fetal germ cells
524 normally display the lowest level of global DNA methylation of any cell type at any developmental stage.
525 This is characteristic of the epigenetic ground state that accrues uniquely in developing germ cells
526 (Hajkova, 2011), and is believed to reflect a generally more accessible chromatin state genome-wide in
527 germ cells than in other cell types. Thus, it may be that the epigenetic ground state in developing germ
528 cells renders this cell type uniquely susceptible to epimutagenesis in gene promoter regions, thereby
529 predisposing a high level of dysregulation of gene expression in response to exposure to an EDC.

530 Finally, our *in vitro* system allowed us to follow the fate of BPS-induced epimutations through a
531 major transition in cell fate from pluripotent to germline cells during which a portion of the normal
532 generational germline epigenetic reprogramming process is known to occur (Kurimoto and Saitou,
533 2018). Thus, when we induced iPSCs previously exposed to 1 µM BPS to differentiate into PGCLCs, we
534 found that a substantial prevalence of epimutations persisted during this transition. However, very few
535 of the specific DMCs or the associated DEGs detected in the BPS-exposed iPSCs persisted in the
536 subsequently derived PGCLCs. Specifically, only 3.7 % of DMCs and 8.4 % of DEGs were conserved
537 between the BPS-exposed iPSCs and the subsequently derived PGCLCs. This suggests that exposure of

538 cells to EDCs has the potential to disrupt epigenetic programming in a way that then interferes with
539 subsequent generational reprogramming that normally accompanies either germline to pluripotent or
540 pluripotent to germline transitions in cell fate. Recent *in vivo* studies have suggested that exposure of
541 gestating female mice to the EDC tributyltin results in disruption not simply of the pattern of epigenetic
542 modifications but also of the underlying chromatin landscape (Chamorro-García et al., 2021; Chang et
543 al., 2022). In this context, our results are consistent with the suggestion that exposure of cells to EDCs
544 can disrupt the underlying chromatin landscape (e.g. the pattern of A and B chromatin compartments)
545 such that when the "normal" reprogramming machinery then acts on this disrupted landscape it
546 corrects many of the originally induced epimutations, but simultaneously induces many novel
547 epimutations *de novo*. This would predispose ongoing abnormalities in the underlying chromatin
548 landscape that would, in turn, lead to the recurring correction of many existing epimutations in concert
549 with the genesis of many novel epimutations during each subsequent generation.

550 Taken together, our results demonstrate the utility of an *in vitro* cell culture approach for
551 pursuing molecular mechanisms underlying environmentally induced disruption of normal epigenetic
552 programming manifest as the formation of epimutations and dysregulated gene expression. This
553 approach clearly affords unique potential to reveal mechanisms responsible for the initial induction of
554 epimutations in response to direct exposure of cells to disruptive effects such as EDCs, as well as
555 offering potential means to elucidate mechanisms by which environmentally induced epimutations are
556 then propagated within the exposed individual and then to that individual's descendants. Knowledge of
557 these mechanisms will afford the best opportunity to understand how these defects may, in the future,
558 be better diagnosed, treated, and/or prevented. With the ever-expanding catalogue of potentially
559 hazardous man-made compounds permeating our environment, it is increasingly important that we
560 recognize the potential dangers such compounds may impose and maximize our ability to protect
561 ourselves from those dangers.

562

563 **Materials and methods**

564 **Key resources table**

Reagent type (species) or resource	Designation	Source or reference	Identifiers	Additional information
Genetic reagent (*M. musculus*)	R26^{rtTA}; Col1a1$^{2lox\text{-}4F2A}$	The Jackson Laboratory	011011	
Cell line (*M. musculus*)	CF1 Mouse embryonic fibroblasts, MitC-treated	Thermo Fisher Scientific	A34959	
Chemical compound	Dulbecco's Modified Eagle Medium (DMEM)	Thermo Fisher Scientific	10313021	High glucose, pyruvate, no glutamine
Chemical compound	Fetal bovine serum (FBS)	Thermo Fisher Scientific	10439024	Embryonic stem-cell FBS, qualified, USDA-approved regions
Chemical compound	Leukemia inhibitory factor (LIF)	Millipore Sigma	ESG1107	ESGRO® Recombinant Mouse LIF Protein
Chemical compound	DMEM/F12	Thermo Fisher Scientific	21041025	No phenol red
Chemical compound	Insulin	Millipore Sigma	I1882	From bovine pancreas
Chemical compound	Apo-Transferrin	Millipore Sigma	T1147	From human
Chemical compound	Bovine Serum Albumin (BSA)	Thermo Fisher Scientific	15260037	Fraction V (7.5% solution)
Chemical compound	Progesterone	Millipore Sigma	P8783	
Chemical compound	Putrescine dihydrochloride	Millipore Sigma	P5780	
Chemical compound	Sodium selenite	Millipore Sigma	S5261	
Chemical compound	Neurobasal™	Thermo Fisher		No phenol red

		Scientific		
Chemical compound	B-27™	Thermo Fisher Scientific	12587010	(50X), minus vitamin A
Chemical compound	Penicillin-streptomycin	Thermo Fisher Scientific	15070063	(5,000 U/mL)
Chemical compound	GlutaMAX™	Thermo Fisher Scientific	35050061	(100X)
Chemical compound	2-Mercaptoethanol	Thermo Fisher Scientific	21985023	(1000X)
Chemical compound	CHIR99021	BioVision	1677-5	
Chemical compound	PD0325901	Amsbio	04-0006-02	10 mM in DMSO
Chemical compound	Recombinant Human/Murine/Rat Activin A	PeproTech	120-14	Insect derived
Chemical compound	Recombinant Human FGF-Basic (FGF-2/bFGF)	Thermo Fisher Scientific	13256-029	
Chemical compound	KnockOut™ Serum	Thermo Fisher Scientific	10828028	
Chemical compound	Glasgow's MEM (GMEM)	Thermo Fisher Scientific	11710035	
Chemical compound	Recombinant human bone morphogenetic protein 4 (BMP-4)	R&D Systems	314-BP-010	
Chemical compound	Recombinant mouse stem cell factor (SCF)	R&D Systems	455-MC-010	
Chemical compound	Recombinant human epidermal growth factor (EGF), carrier free (CF)	R&D Systems	2028-EG-200	
Chemical compound	Dulbecco's phosphate-buffered saline (DPBS)	Thermo Fisher Scientific	14040133	
Chemical compound	Deoxyribonuclease I (DNaseI)	Millipore Sigma	DN25	From bovine pancreas
Chemical compound	Trypsin (2.5%)	Thermo Fisher Scientific	15090046	No phenol red
Chemical	Soybean trypsin	Thermo	17075029	

compound	inhibitor	Fisher Scientific		
Chemical compound	Collagenase type IV	Worthington	LS004188	From *Clostridium histolyticum*
Chemical compound	Sertoli Cell Medium	ScienCell Research Laboratories	4521	
Chemical compound	Ethanol (EtOH)	Fisher	BP28184	(200 Proof)
Chemical compound	BSA	Millipore Sigma	A9085	
Chemical compound	Heat inactivated (HI) FBS	Thermo Fisher Scientific	10082147	
Chemical compound	Trypsin-EDTA (0.25%)	Thermo Fisher Scientific	25200072	With phenol red
Chemical compound	Bisphenol S (BPS)	Millipore Sigma	43034-100MG	
Chemical compound	Phenol:Chloroform:Isoamyl Alcohol (25:24:1, v/v)	Thermo Fisher Scientific	15593031	
Chemical compound	TRIzol™	Thermo Fisher Scientific	15596026	
Chemical compound	Isopropanol	Thermo Fisher Scientific	327272500	
Chemical compound	Proteinase K Solution (20 mg/mL)	Thermo Fisher Scientific	25530049	
Chemical compound	MaXtract High Density	Quiagen	129046	Phase lock gel tubes
Chemical compound	Sodium Acetate Solution	Thermo Fisher Scientific	R1181	3M, pH 5.2
Chemical compound	Glycogen (5 mg/ml)	Thermo Fisher Scientific	AM9510	
Chemical compound	NaCl	Thermo Fisher Scientific	J21618.36	
Chemical compound	Tris base	Millipore Sigma	77-86-1	
Chemical compound	Ethylenediaminetetra acetic acid (EDTA)	Millipore Sigma	E9884-100G	
Chemical	Sodium dodecyl	Millipore	151-21-3	

compound	sulfate (SDS)	Sigma		
Chemical compound	Triton X-100	Thermo Fisher Scientific	85111	
Chemical compound	RQ1 DNase	Promega	M6101	
Chemical compound	Propidium iodide	BioLegend	421301	FCy 5 µL/10^6 cells
Antibody	ERα	Thermo Fisher Scientific	MA1-310	Host: mouse, ICC 1:100
Antibody	ERβ	GeneTex	GTX70174	Host: mouse, ICC 1:100
Antibody	INHA	Invitrogen	PA5-13681	Host: rabbit, ICC 1:25
Antibody	FSHR	Affinity	AF5477	Host: rabbit, ICC 1:250
Antibody	SOX9	Abcam	ab185966	Host: rabbit, ICC 1:100
Antibody	GAPDH	Novus	NB300-221	Host: mouse, ICC 1:100
Antibody	WT1	Novus	NBP2-67587	Host: rabbit, ICC 1:100
Antibody	FUT4	GeneTex	GTX34467	Host: rabbit, ICC 1:50
Antibody	NANOG	Abcam	ab80892	Host: rabbit, ICC 1:100
Antibody	POU5F1	Abcam	ab19857	Host: rabbit, ICC 1:200
Antibody	SOX2	Abcam	ab97959	Host: rabbit, ICC 1:200
Antibody	ID4	Thermo Fisher Scientific	PA5-26976	Host: rabbit, ICC 1:50
Antibody	Goat Anti Mouse Alexa 488	Abcam		Host: goat, ICC 1:1000
Antibody	Goat Anti Rabbit Alexa 647	Abcam	ab150199	Host: goat, ICC 1:200
Antibody	FUT4 (IgM, κ), brilliant violet 421	BioLegend	125614	Host: mouse, FCy 5 µL/10^6 cells
Antibody	ITGB3 (IgG), PE	BioLegend	104307	Host: hamster, FCy 1 µL/10^6 cells
Antibody	IgM, κ Isotype control, brilliant violet 421	BioLegend	562704	Host: mouse, FCy 1.25 µL/10^6 cells
Antibody	IgG Isotype control, PE	BioLegend	400907	Host: hamster, FCy 1 µL/10^6 cells
Commercial	RNA Clean &	Zymo	R1016	

assay or kit	Concentrator-5	Research		
Commercial assay or kit	Genomic DNA Clean & Concentrator-10	Zymo Research	D4011	
Commercial assay or kit	EZ DNA Methylation Kit	Zymo Research	D5001	
Commercial assay or kit	SuperScript™ III One-Step RT-PCR System with Platinum™ Taq DNA Polymerase	Thermo Fisher Scientific	12574026	
Commercial assay or kit	PowerTrack™ SYBR Green Master Mix for qPCR	Thermo Fisher Scientific	A46109	
Commercial assay or kit	Infinium Mouse Methylation BeadChip	Illumina	20041558	
Commercial assay or kit	RNA ScreenTape & Reagents	Agilent	5067-5576	
Commercial assay or kit	DNA ScreenTape & Reagents	Agilent	5067-5583	
Commercial assay or kit	Qubit dsDNA (Broad Range) BR Assay Kit	Thermo Fisher Scientific	Q32850	
Commercial assay or kit	Qubit RNA (high sensitivity) HS Assay Kit	Thermo Fisher Scientific	Q32855	
Commercial assay or kit	NEBNext® Ultra™ II Directional RNA Library Prep Kit for Illumina®	New England BioLabs	E7765	
Commercial assay or kit	NEBNext® Poly(A) mRNA Magnetic Isolation Module	New England BioLabs	E3370	
Software, algorithm	ZEISS ZEN Microscopy Software	https://www.zeiss.com/microscopy/en/products/software/zeiss-zen.html	ZEN 3.7	
Software, algorithm	Primer-BLAST	https://www.ncbi.nlm.nih.gov/tools/primer-blast/		
Software, algorithm	QuantSudtio™ Design & Analysis Software	https://www.thermofisher.com/us/en/home/technical-resources/so	QuantSudtio™ v1.5.1	

		ftware-downloads/quantstudio-3-5-real-time-pcr-systems.html		
Software, algorithm	Fiji	https://fiji.sc/	Fiji v1.54f	(Schindelin et al., 2012)
Software, algorithm	Bfastq2	https://support.illumina.com/downloads/bcl2fastq-conversion-software-v2-20.html	Bcl2fastq2 v2.20	
Software, algorithm	FastQC	https://www.bioinformatics.babraham.ac.uk/projects/fastqc/	FastQC 0.12.0	(Andrews et al., 2023; Smith and de Sena Brandine, 2021)
Software, algorithm	Wg-blimp	https://github.com/MarWoes/wg-blimp	Wg-blimp v0.10.0	(Lehle and McCarrey, 2023; Wöste et al., 2020)
Software, algorithm	R-Project for Statistical Computing	http://www.r-project.org/	R 4.2.1	Packages: Sesame (Ding et al., 2023; Triche et al., 2013; Zhou et al., 2022, 2018), stringr (Wickham and RStudio, 2022), kintr (Xie et al., 2023), SummarizedExperiment (Morgan et al., 2023), ggrepel (Slowikowski et al., 2023), pals (Wright, 2023), wheatmap (Zhou, 2022), tidyr (Wickham et al., 2023) magrittr (Bache et al., 2022), dplyr (Wickham et al., 2023), ggplot2 (Wickham et al., 2023),

				ggvenn (Yan, 2023), RColorBrewer (Neuwirth, 2022), RIdeogram (Hao et al., 2020), AnnotationDbi (Pagès et al., 2023), Mus.musculus (Team BC, 2015), BSgenome.Mmusculus.UCSC.mm10 (Team TBD, 2021), GenomicRanges (Lawrence et al., 2013), universalmotif (Tremblay, 2023), memes (Nystrom, 2023), Plyranges (Lee et al., 2019), rtracklayer (Lawrence et al., 2009), Rsubread (Liao et al., 2019), edgeR (Chen et al., 2016; McCarthy et al., 2012; Robinson et al., 2010)

565

566 **Animal procedures**

567 Mice were used as the primary source of cells for the establishment of cultures for the analysis
568 of differential cell type-specific susceptibility to exposure to the EDC BPS at the cellular level. All mice
569 were euthanized prior to dissection and isolation of the tissue or cell type to be used for experiments.
570 All animals were maintained in one of the UTSA on-campus vivaria and housed under controlled
571 temperature and humidity conditions in a fixed 12-hour light, 12-hour dark cycle with free access to
572 food and water. Euthanasia was performed by trained personnel using continuous CO_2 exposure at a
573 rate of 3L/min until one minute after breathing had stopped. Euthanasia was confirmed by cervical
574 dislocation. Tissue from euthanized mice was used to obtain somatic (Sertoli, granulosa, and mouse
575 embryonic fibroblast [MEF]) cells, and primordial germ cells [PGCs]. Both Sertoli and granulosa cells

576 were isolated from respective male and female mice euthanized at postnatal day 20 (P20). MEFs and
577 PGCs were isolated from fetuses at embryonic day 13.5 postcoitum (E13.5).

578 ***In vitro* generation and/or culture of pluripotent, somatic, and germ cells**

579 **Pluripotent cell culture**

580 Male mouse iPSCs were derived from a transgenic mouse line carrying the *tetO-4F2A* cassette
581 obtained from The Jackson Laboratories (011011) (The Jackson Laboratory, ME USA). iPSCs can be
582 induced from essentially any cell type carrying this reprogrammable cassette by exposure to Doxycycline
583 for one week as previously described (Carey et al., 2010; Hochedlinger et al., 2005). For this project,
584 iPSCs were reprogrammed from MEFs isolated from a single male (XY) E13.5 mouse fetus.
585 Reprogrammed colonies were picked and expanded via sub-passaging. Validation of reprogrammed
586 pluripotency was determined by positive immunocytochemical (ICC) staining for the pluripotent markers
587 POU5F1, SOX2, NANOG, and FUT4 (Supplementary file 1c and 1f). Karyotyping was done on each
588 candidate iPSC line produced to confirm normal chromosome number and XY sex chromosome
589 constitution of each line prior to aliquots being prepared for long-term storage in liquid nitrogen
590 (Supplementary file 1d). Only male (XY) iPSC lines were used for this project. Upon thawing, iPSCs were
591 initially maintained on CF-1 feeder cells for a minimum of three passages. Cells were cultured in DMEM
592 supplemented with 15% fetal bovine serum (FBS) and 1000 U/mL leukocyte inhibitory factor (LIF). Once
593 pluripotent cells were stabilized in culture, they were transitioned to feeder-free conditions and were
594 cultured in N2B27 media supplemented with 2i and LIF for two-three passages prior to use in chemical
595 exposure experiments. A complete list of the media components along with catalog numbers can be
596 found in Supplementary file 1e.

597 **Sertoli cell culture**

598 Primary cultures of Sertoli cells were established as previously described (Karl and Griswold,
599 1990). Briefly, whole testes were dissected from juvenile mice at P20. Following removal of the tunica
600 albuginea from each individual testis, the bundles of seminiferous tubules were physically chopped
601 using a sterile razor blade to break down the coiled structure of tubules increasing the surface area and
602 rendering them easier to digest. These shortened fragments of seminiferous tubules were then digested
603 in a mixture of 2.5% trypsin and 6.64 mg/ml DNaseI in DPBS for 25 minutes at 37°C. After these enzymes
604 were inactivated, the tubule sections were washed multiple times, then treated with a final enzymatic
605 mixture of collagenase IV (0.70 mg/mL) and DNaseI (6.64 mg/mL) for 10 minutes to permeabilize the
606 thick collagen layer on the exterior of the seminiferous tubules to allow the Sertoli cells to migrate out
607 away from the tubules in culture. After checking the digested tubules under a microscope to confirm the
608 collagen layer had been permeabilized, the digested tubules were spun down to wash away the
609 enzymes, and then plated in Sertoli cell media containing retinoic acid from ScienCell^{TM} (4521)
610 (ScienCell^{TM} Research Laboratories, CA USA). To remove contaminating germ cells from this primary
611 culture, the cells were treated with hypotonic shock treatment on the morning of the second day of
612 culture, and the enriched Sertoli cells were washed and allowed to recover with fresh media for at least
613 two hours. The enriched primary cultures of Sertoli cells were then ready to be used for chemical
614 exposure experiments. The estimated purity of the culture was > 80% based on ICC staining for the
615 Sertoli cell marker SOX9 and WT1 (Supplementary file 1f). A full procedure for the establishment of
616 primary cultures of Sertoli cells can be found in Supplementary file 1g.

617 **Granulosa cell culture**

618 Primary cultures of granulosa cells were established by selecting early preantral primary follicles
619 from enzymatically digested ovary tissue as described previously (Monti and Redi, 2016; Roy and
620 Greenwald, 1996), followed by breaking selected primary follicles down into a single cell suspension that
621 could be plated and maintained. To isolate preantral primary follicles we dissected ovaries from female

622 mice at P20 and then enzymatically digested the ovary using collagenase IV (560 U/pair of ovaries) for
623 25 minutes at 37°C with constant agitation. This digestion was stopped by addition of buffer with 0.5%
624 BSA and the mixture was spun down at 60xg for 5 minutes to pellet the cells. The cells were
625 resuspended in PBS with 0.5% BSA and transferred to a sterile petri dish under a stereomicroscope.
626 Primary follicles were individually picked from the solution using a glass needle with suction control and
627 moved into a clean droplet of PBS containing 0.5% BSA. Selected primary follicles were then spun down
628 at 1000xg for 5 mins. After spinning, the supernatant was removed, and the cells were finger-vortexed
629 to resuspend the pellet. The follicles were then digested to single cell suspension by addition of pre-
630 warmed (37°C) 0.25% trypsin and incubated for 5 mins with regular pipetting followed by pelleting again
631 at 1000xg for 5 mins. The trypsin-containing supernatant was removed, and the granulosa cells were
632 resuspended in DMEM supplemented with 15% FBS and plated for maintenance in culture. The oocytes
633 were non-adherent and were washed away on day 2 when changing the media. The estimated purity of
634 the culture was > 90% based on ICC staining for the granulosa cell marker FSHR and INHA
635 (Supplementary file 1f). The granulosa cells were then ready to be used for EDC exposure experiments.
636 A full procedure for the establishment of primary cultures of granulosa cells can be found in
637 Supplementary file 1h.

638 **Primordial germ cell like cell culture**

639 Mouse iPSCs were differentiated into PGCLCs as previously described (Hayashi et al., 2011).
640 Briefly, iPSCs maintained in N2B27 supplemented with 2i and LIF under feeder free conditions were
641 differentiated to EpiLCs for two days by the addition of activin A and basic fibroblast growth factor
642 (bFGF) to the N2B27 media. After two days the EpiLC intermediate cells were passaged to low
643 adherence round bottom plates for 4 days in GK15 media containing bone morphogenic protein 4
644 (BMP4), stem cell factor (SCF), epidermal growth factor (EGF), and LIF to induce the differentiation of a
645 subset of cells (2-3%) in the resulting aggregate to become PGCLCs. During this four-day period, cell

646 aggregates were ready for EDC exposure (see below). Following EDC exposure, cell aggregates were
647 removed from the low adherence round bottom plates, dissociated into a single cell suspension, and
648 PGCLCs were fluorescence-activated cell sorted (FACS) on a BD FACSAria™ II in the UTSA Cell Analysis
649 Core to recover cells that were double-positive for FUT4 and ITGB3. A full list of the media components
650 and catalog numbers for the differentiation of iPSCs to PGCLCs along with our FACS gating for double
651 positive FUT/ITGB3 PGCLCs can be found in Supplementary file 1e and 1i, respectively. Additional data
652 demonstrating validation of PGCLCs by qRT-PCR and ICC staining are shown in Supplementary file 1j.

653 **Immunocytochemistry (ICC)**

654 Cells were immunolabeled as previously described (Rodig, 2022) to validate the purity of cell
655 primary cultures using known cell specific markers (Supplementary file 1f) detect the presence or
656 absence of relevant endocrine receptors ERα and ERβ at the protein level. Pluripotent (iPS) and somatic
657 (Sertoli and granulosa) cells were grown on 13mm Thermanox® plastic coverslips (174950) prior to
658 fixation, permeabilization, and immunolabeling (Nalge Nunc International, NY USA). Non-adherent germ
659 (PGC and PGCLC) cells were spun down onto poly-L-lysine coated slides (63410-01) at 400 RPM for one
660 minute using a Thermo Shandon CytoSpin III Cytocentrifuge from Rakin (Electron Microscopy Sciences,
661 PA USA & Rakin Biomedical Corporation, MI USA). Cells were fixed with 4% formaldehyde for 10 mins at
662 room temp (RT) and then washed three times for five minutes each with ICC buffer (PBS containing
663 0.01% Triton X-100 detergent) to permeabilize the cell and nuclear membranes prior to blocking with 5%
664 goat serum which was added to the ICC buffer and incubated for one hour at RT. Following blocking,
665 primary antibodies, in ICC buffer, were added to the slides and left to incubate overnight at 4°C. The
666 following day, slides were washed three times with ICC buffer, and fluorescent secondary antibodies in
667 ICC buffer were then added to the slides and left to incubate in the dark for 1 hour. After secondary
668 antibody incubation, cellular nuclei were stained with DAPI at a 1:1000 dilution in ICC buffer for 7
669 minutes, followed by 3 final washes with ICC buffer for 5 minutes. Coverslips then were transferred to

670 microscope slides and mounted with 5-10 µL of VECTASHEILD Antifade Mounting Medium (H-1000) and
671 sealed with clear nail polish before being imaged on a Zeiss AXIO Imager.M1 Fluorescence Microscope
672 (Vector Laboratories Inc, CA USA & Zeiss Group, Oberkochen DE). Images were processed for contrast
673 and brightness enhancement and for the addition of scale bars using Fiji (Schindelin et al., 2012).
674 Information about the primary and secondary antibodies along with catalogue numbers and dilutions
675 used can be found in the Key resources table.

676 **Quantitative RT-PCR (qRT-PCR)**

677 Total RNA was extracted from cells as described previously (Rio et al., 2010) and treated with 1.5
678 U/µg total RNA RQ1 DNase1 (M6101) to remove contaminating genomic DNA (Promega™ Corporation,
679 WI USA). 50 ng of cleaned RNA was retrotranscribed with SuperScript™ III as recommended by the
680 manufacturer (Invitrogen, MA USA). Primers were designed using Primer-BLAST (Ye et al., 2012) from
681 NCBI. A complete list of all primer sequences used in this study can be found in Supplementary file 1j.
682 Relative expression levels of selected genes were assessed by real-time PCR using the PowerTrack™
683 SYBR Green Master Mix according to the manufacturer's instructions (Applied Biosystems, MA USA)
684 then run on a QuantStudio™ 5 Real-Time PCR System (Thermo Fisher Scientific, MA USA) and analyzed
685 with QuantStudio™ Design & Analysis Software. Each sample was normalized based on constitutive
686 expression of the *Gusb* reference gene to obtain the ΔCt [(2-[Ctgene-CtGusb)].

687 **BPS exposure design**

688 Despite numerous studies illustrating the dangers of estrogenic mimetic EDCs, the EPA has
689 currently not published any limits concerning the maximum acceptable dose of BPS below which
690 exposure on a daily basis is considered to be safe. Thus for this study, we established our initial testing
691 range of 1 µM, 50 µM, and 100 µM of BPS based on the limit established for BPA at ≤ 4.44 µM (Ribeiro
692 et al., 2019) selecting 1 dose below the established safe limit and two doses that exceed that limit. For

693 all cell types except PGCLCs, BPS was added to media gassed with 5% CO_2, 5% O_2, and balanced N_2 and
694 then injected into sealed T-25 cell culture flasks and left to incubate for 24 hours (Supplementary file
695 1k). The media was gassed to ensure enrichment to 5% CO_2, which is normally regulated by the cell
696 incubator, limiting the potential for the pH to change in the media during this exposure period due to
697 the absorption of CO_2 by incubating cells. Following 24 hours of exposure, media containing BPS was
698 removed and cells were washed and allowed to recover in fresh untreated media (without BPS or EtOH)
699 for 24 hours prior to harvesting. PGCLCs were not suitable for this exposure paradigm as EpiLCs undergo
700 differentiation to PGCLCs in cell aggregates formed in low-adherence round-bottom 96 well plates and
701 cannot be maintained in T-25 sealed flasks. Therefore, diluted BPS was added to PGCLC media and
702 added to cells in round-bottom 96 well plates to incubate for 24 hours prior to a shortened wash and
703 "chase" period of 8 hours prior to cell sorting.

704 **Methylation beadchip analysis**

705 A total of 1µg of extracted genomic DNA was bisulfite-converted with the EZ DNA Methylation
706 Kit (D5001) and modified according to the manufacturer's recommendations (Zymo Research, CA USA &
707 Illumina, CA USA). These samples were run on the Infinium Mouse Methylation BeadChip Array
708 following the Illumina Infinium HD Methylation protocol. This beadchip array includes 297,415 cytosine
709 positions within the mouse genome (CpG sites, non-CpG sites, and random SNPs). The methylation score
710 for each CpG is represented as a β-value which is a ratio of the fluorescence intensity ranging between 0
711 (unmethylated) and 1 (methylated). Arrays were scanned by HiScan (Illumina, CA USA). Quality control
712 (Supplementary file 1m) and downstream data processing of the .idat files was using the Sensible Step-
713 wise Analysis of DNA Methylation BeadChips (SeSAMe) Bioconductor package (Ding et al., 2023; Triche
714 et al., 2013; Zhou et al., 2022, 2018). DNA methylation levels of differentially methylated cytosines
715 (DMCs) are determined using mixed linear models. This general supervised learning framework
716 identifies CpG loci whose differential methylation is associated with known control vs. treated co-

717 variates. CpG probes on the array were defined as having differential changes that met both p-value and
718 FDR ≤ 0.05 significant thresholds between treatment and control samples for each cell type analyzed.
719 Additionally, we followed up our DNA methylation analysis of individual dCpGs by identifying
720 differentially methylated regions (DMRs). DMRs were created by grouping all CpGs measured on the
721 array into clusters using Euclidean distance (Ding et al., 2023; Triche et al., 2013; Zhou et al., 2022,
722 2018). The p-values from the differential methylation of individual CpGs within the resulting CpG
723 clusters were aggregated, and clusters were then filtered selecting for regions that contained a p-value ≤
724 0.05 (Ding et al., 2023; Triche et al., 2013; Zhou et al., 2022, 2018).

725 **RNA-seq**

726 Total RNA was extracted from cells using Trizol as previously described (Rio et al., 2010).
727 Contaminating genomic DNA was removed by RQ1 DNase (M6101) treatment according to the
728 manufacturer's instructions (Promega Corporation, WI USA). RNA concentration was determined using
729 Qubit (Q32855) and RNA integrity (RIN) scores were determined using tape station (5067-5576)
730 according to the manufacturer's instructions (Thermo Fisher Scientific Inc, MA USA & Agilent
731 Technologies, Inc CA USA). Strand-specific RNA-seq libraries were prepared with the NEBNext® Ultra™ II
732 Directional RNA Library Prep Kit for Illumina® sequencing (E7760S) according to the manufacturer's
733 protocol (New England Biolabs, MA USA). Briefly, this process consisted of poly(A) RNA selection, RNA
734 fragmentation, and double stranded cDNA generation using random oligo(dT) priming followed by end
735 repair to generate blunt ends, adaptor ligation, strand selection, and polymerase chain reaction
736 amplification to generate the final library. Distinct index adaptors were used for multiplexing samples
737 across multiple sequencing lanes. Sequencing was performed on an Illumina NovaSeq 6000 instrument
738 yielding sequences of paired end 2x50 base pair runs. Demultiplexing was performed with the Illumina
739 Bcl2fastq2 program (Illumina, CA USA).

740 **RNA-seq expression analysis**

741 The quality of the fastq reads was checked using FastQC (Andrews et al., 2023; Smith and de
742 Sena Brandine, 2021) (Supplementary file 1n). Reads were aligned to the mm10 mouse reference
743 genome using the Rsubreads package to produce read counts (Liao et al., 2019). These were then used
744 for differential gene expression analysis using the edgeR package (Chen et al., 2016; McCarthy et al.,
745 2012; Robinson et al., 2010). Briefly, gene counts were normalized using the trimmed mean of M-value
746 normalization (TMM) method before determining counts per million (CPM) values (Robinson and
747 Oshlack, 2010). For a gene to be classified as showing differential gene expression between BPS-treated
748 and EtOH vehicle-only control samples, a threshold of both a Benjamini-Hochberg adjusted p-value ≤
749 0.05 and a false discovery rate (FDR) ≤ 0.05 had to be met.

750 **EM-Seq**

751 Genomic DNA was extracted from cells as previously described (Sambrook and Russell, 2006).
752 Smaller fragmented DNA (≤ 10 kb) and contaminating RNA were removed by cleaning the genomic DNA
753 on a genomic DNA clean and concentrator™-10 column (D4011), according to the manufacturer's
754 instructions (Zymo Research, CA USA). DNA concentration was determined using a Qubit (Q32850) and
755 genomic DNA (100 ng) was sheered using a Bioruptor® and the size of the sheered DNA was determined
756 using a TapeStation 4200 according to the manufacturer's instructions in the UTSA Genomics Core
757 (Diagenode Inc, NJ USA & Agilent Technologies, Inc CA USA). Large size (470-520 bp) EM-seq libraries
758 were prepared with the NEBNext® Enzymatic Methyl-seq kit (E7120S) according to the manufacturer's
759 protocol (New England Biolabs, MA USA). Briefly, this process consisted of A-tailing, adaptor ligation,
760 DNA oxidation by TET2 initiated by the addition of Fe (II), strand denaturization with formamide,
761 deamination by APOBEC3A, polymerase chain reaction amplification, and bead selection to generate the
762 final libraries. Distinct index adaptors were used for multiplexing samples across multiple sequencing

763 lanes. Sequencing was performed on an Illumina NovaSeq 6000 instrument yielding sequences of paired
764 end 2x150 base pair runs. Demultiplexing was performed with the Illumina Bcl2fastq2 program
765 (Illumina, CA USA).

766 **EM-Seq analysis of genome-wide DNA methylation patterns**

767 EM-seq data was processed using the comprehensive wg-blimp v10.0.0 software pipeline (Lehle
768 and McCarrey, 2023; Wöste et al., 2020). In brief, reads were trimmed prior to initiating the wg-blimp
769 pipeline using Trim Galore (https://www.bioinformatics.babraham.ac.uk/projects/trim_galore/).
770 Sequenced reads were aligned to the mm10 genome using gemBS (King et al., 2020; Merkel et al., 2019;
771 Schilbert et al., 2020). The BAM files from alignment underwent a series of QC tests including read
772 quality scoring by FastQC (Andrews et al., 2023), overall and per-chromosome read coverage calculation,
773 GC content, duplication rate, clipping profiles by Qualimap (Okonechnikov et al., 2016), and
774 deduplication by the Picard toolkit (https://broadinstitute.github.io/picard/) (Supplementary file 1o).
775 Methylation calling was performed by MethylDackel (https://github.com/dpryan79/MethylDackel) and
776 statistically significant DMC/DMR calling was performed by the metilene (Jühling et al., 2016) and
777 BSmooth (Hansen et al., 2012) algorithms. Metilene uses a binary segmentation algorithm combined
778 with a two-dimensional statistical test that allows the detection of DMCs/DMRs in large methylation
779 experiments with multiple groups of samples. BSmooth uses a local-likelihood approach to estimate a
780 sample-specific methylation profile, then computes estimates of the mean differences and standard
781 errors for each CpG to form a statistic similar to that used in a t-test. Finally, potential regulatory regions
782 were identified through the use of MethylSeekR (Burger et al., 2013). Results from the pipeline were
783 displayed in the wg-blimp interactive results web browser that was built using the R Shiny local browser
784 hosting framework (Chang et al., 2023).

785

786 **Data availability**

787 Methylation beadchip, EM-seq, and RNA-seq data discussed in this publication can be obtained from the
788 SRA BioProject (PRJNA1026145).

789 **Article and author information**

790 **Author details**

791 1. **Jake D. Lehle**

792 • Department of Neuroscience, Developmental and Regenerative Biology, The University
793 of Texas at San Antonio, Texas, United States of America

794 **Contribution:** Conceptualization, Data curation, Software, Formal analysis, Validation,
795 Investigation, Visualization, Methodology, Writing – original draft

796 **Competing interests:** No competing interests declared

797 **ORCiD:** 0000-0002-0833-7068

798

799 2. **Yu-Huey Lin**

800 • Department of Neuroscience, Developmental and Regenerative Biology, The University
801 of Texas at San Antonio, Texas, United States of America

802 **Contribution:** Data curation, Formal analysis, Validation, Investigation, Visualization,
803 Methodology

804 **Competing interests:** No competing interests declared

805 **ORCiD:** 0009-0003-1321-0680

806

807 **3. Amanda Gomez**

808 • Department of Biomedical Engineering and Chemical Engineering, The University of
809 Texas at San Antonio, Texas, United States of America

810 **Contribution:** Data curation, Software, Investigation, Visualization

811 **Competing interests:** No competing interests declared

812 **ORCiD:** 0000-0002-0767-1275

813

814 **4. Laura Chavez**

815 • Department of Neuroscience, Developmental and Regenerative Biology, The University
816 of Texas at San Antonio, Texas, United States of America

817 **Contribution:** Data curation, Investigation, Visualization

818 **Competing interests:** No competing interests declared

819 **ORCiD:** 0000-0001-6174-0430

820

821 **5. John R. McCarrey**

822 • Department of Neuroscience, Developmental and Regenerative Biology, The University
823 of Texas at San Antonio, Texas, United States of America

824 **Contribution:** Conceptualization, Supervision, Funding acquisition, Project administration

825 **For correspondence:** John.McCarrey@utsa.edu

Competing interests: No competing interests declared

ORCiD: 0000-0002-5784-9318

Funding

National Institute of Health

NICHD P50 (HD98593)

- John R. McCarrey

National Institute of Health

NIDA (U01DA054179)

- John R. McCarrey

Robert J. and Helen C. Kleberg Foundation

- John R. McCarrey

Nancy Hurd Smith Foundation

- John R. McCarrey

Acknowledgments

This work was supported by grants from the NIH to JRM (HD98593 and DA054179), and gifts from the Robert J. Kleberg, Jr. and Helen C. Kleberg Foundation and the Nancy Hurd Smith Foundation. The authors would like to thank: Michael Klein and the Genomics Core Facility and staff at the University of Utah for their assistance with processing the Illumina Infinium Mouse Methylation Beadchip Array

846 samples; Sean Vargas at the UTSA Genomics core for his expertise and supervision for utilizing
847 equipment to prepare sequencing libraries; Dr. Sandra Cardona at the UTSA Cell Analysis Core for her
848 expertise and supervision performing FACS to isolate cells; Dr. Brian Herman for use of his fluorescent
849 microscope for the collection of images; and Dr. Brian Bringham for biostatistics advice. This work
850 received computational support from UTSA's HPC cluster Arc, operated by Tech Solutions. Sequencing
851 data in this study was generated at the UT Health Genome Sequencing Facility, which is supported by UT
852 Health San Antonio, NIH-NCI P30 CA054174 (Cancer Center at UT Health San Antonio) and NIH Shared
853 Instrument grant S10OD030311 (S10 grant to NovaSeq 6000 System), and CPRIT Core Facility Award
854 (RP220662).

855

856 **Ethics**

857 All experimental procedures involving animals were approved in advance by the UTSA IACUC (Protocols
858 MU015 and MU016).

859

860

861

862

863 **References:**

864 Almeida M, Pintacuda G, Masui O, Koseki Y, Gdula M, Cerase A, Brown D, Mould A, Innocent C,
865 Nakayama M, Schermelleh L, Nesterova TB, Koseki H, Brockdorff N. 2017. PCGF3/5-PRC1 initiates
866 Polycomb recruitment in X chromosome inactivation. *Science (80-)* **356**:1081–1084.
867 doi:10.1126/science.aal2512

868 Andrews S, Krueger F, Segonds-Pichon A, Biggins L, Krueger C, Montgomery J. 2023. Babraham
869 Bioinformatics - FastQC A Quality Control tool for High Throughput Sequence Data.

870 Anway MD, Leathers C, Skinner MK. 2006. Endocrine disruptor vinclozolin induced epigenetic
871 transgenerational adult-onset disease. *Endocrinology* **147**:5515–5523. doi:10.1210/en.2006-0640

872 Bache S, Wickham H, Henry L, Rstudio. 2022. magrittr: A Forward-Pipe Operator for R.

873 Bao M, Cornwall-Scoones J, Sanchez-Vasquez E, Chen DY, De Jonghe J, Shadkhoo S, Hollfelder F,
874 Thomson M, Glover DM, Zernicka-Goetz M. 2022. Stem cell-derived synthetic embryos self-
875 assemble by exploiting cadherin codes and cortical tension. *Nat Cell Biol* **24**:1341–1349.
876 doi:10.1038/S41556-022-00984-Y

877 Beamish SB, Frick KM. 2022. A Putative Role for Ubiquitin-Proteasome Signaling in Estrogenic Memory
878 Regulation. *Front Behav Neurosci* **15**:807215. doi:10.3389/FNBEH.2021.807215/BIBTEX

879 Bourdeau V, Deschênes J, Métivier R, Nagai Y, Nguyen D, Bretschneider N, Gannon F, White JH, Mader S.
880 2004. Genome-Wide Identification of High-Affinity Estrogen Response Elements in Human and
881 Mouse. *Mol Endocrinol* **18**:1411–1427. doi:10.1210/ME.2003-0441

882 Brenker C, Rehfeld A, Schiffer C, Kierzek M, Kaupp UB, Skakkebæk NE, Strünker T. 2018. Synergistic
883 activation of CatSper Ca2+ channels in human sperm by oviductal ligands and endocrine disrupting
884 chemicals. *Hum Reprod* **33**:1915–1923. doi:10.1093/humrep/dey275

885 Burger L, Gaidatzis D, Schübeler D, Stadler MB. 2013. Identification of active regulatory regions from
886 DNA methylation data. *Nucleic Acids Res* **41**:e155–e155. doi:10.1093/NAR/GKT599

887 Cantone I, Fisher AG. 2013. Epigenetic programming and reprogramming during development. *Nat*
888 *Struct Mol Biol*. doi:10.1038/nsmb.2489

889 Carey BW, Markoulaki S, Beard C, Hanna J, Jaenisch R. 2010. Single-gene transgenic mouse strains for
890 reprogramming adult somatic cells. *Nat Methods* **7**:56–59. doi:10.1038/NMETH.1410

891 Chamorro-García R, Poupin N, Tremblay-Franco M, Canlet C, Egusquiza R, Gautier R, Jouanin I, Shoucri
892 BM, Blumberg B, Zalko D. 2021. Transgenerational metabolomic fingerprints in mice ancestrally
893 exposed to the obesogen TBT. *Environ Int* **157**. doi:10.1016/J.ENVINT.2021.106822

894 Chang RC, Egusquiza RJ, Huang Y, Amato AA, Joloya EM, Wheeler HB, Nguyen A, Shioda K, Odajima J,
895 Shioda T, Blumberg B. 2022. Heritable changes in chromatin contacts linked to transgenerational
896 obesity. *bioRxiv* 2022.10.27.514145. doi:10.1101/2022.10.27.514145

897 Chang W, Cheng J, Allaire J, Sievert C, Schloerke B, Xie Y, Allen J, McPherson J, Dipert A, Borges B,
898 Software P, PBC. 2023. shiny: Web Application Framework for R.

899 Chen Y, Lun ATL, Smyth GK, Burden CJ, Ryan DP, Khang TF, Lianoglou S. 2016. From reads to genes to
900 pathways: differential expression analysis of RNA-Seq experiments using Rsubread and the edgeR
901 quasi-likelihood pipeline. *F1000Research 2016 51438* **5**:1438. doi:10.12688/f1000research.8987.2

902 Davaapil H, Shetty DK, Sinha S. 2020. Aortic "Disease-in-a-Dish": Mechanistic Insights and Drug
903 Development Using iPSC-Based Disease Modeling. *Front Cell Dev Biol* **8**.
904 doi:10.3389/FCELL.2020.550504

905 Deb P, Bhan A, Hussain I, Ansari KI, Bobzean SA, Pandita TK, Perrotti LI, Mandal SS. 2016. Endocrine
906 disrupting chemical, bisphenol-A, induces breast cancer associated gene HOXB9 expression in vitro

907 and in vivo. *Gene* **590**:234–243. doi:10.1016/j.gene.2016.05.009

908 Diaz-Castillo C, Chamorro-Garcia R, Shioda T, Blumberg B. 2019. Transgenerational Self-Reconstruction
909 of Disrupted Chromatin Organization After Exposure To An Environmental Stressor in Mice. *Sci*
910 *Reports 2019 91* **9**:1–15. doi:10.1038/s41598-019-49440-2

911 Ding W, Kaur D, Horvath S, Zhou W. 2023. Comparative epigenome analysis using Infinium DNA
912 methylation BeadChips. *Brief Bioinform* **24**. doi:10.1093/BIB/BBAC617

913 Dunham I, Kundaje A, Aldred SF, Collins PJ, Davis CA, Doyle F, Epstein CB, Frietze S, Harrow J, Kaul R,
914 Khatun J, Lajoie BR, Landt SG, Lee BK, Pauli F, Rosenbloom KR, Sabo P, Safi A, Sanyal A, Shoresh N,
915 Simon JM, Song L, Trinklein ND, Altshuler RC, Birney E, Brown JB, Cheng C, Djebali S, Dong X, Ernst
916 J, Furey TS, Gerstein M, Giardine B, Greven M, Hardison RC, Harris RS, Herrero J, Hoffman MM, Iyer
917 S, Kellis M, Kheradpour P, Lassmann T, Li Q, Lin X, Marinov GK, Merkel A, Mortazavi A, Parker SCJ,
918 Reddy TE, Rozowsky J, Schlesinger F, Thurman RE, Wang J, Ward LD, Whitfield TW, Wilder SP, Wu
919 W, Xi HS, Yip KY, Zhuang J, Bernstein BE, Green ED, Gunter C, Snyder M, Pazin MJ, Lowdon RF,
920 Dillon LAL, Adams LB, Kelly CJ, Zhang J, Wexler JR, Good PJ, Feingold EA, Crawford GE, Dekker J,
921 Elnitski L, Farnham PJ, Giddings MC, Gingeras TR, Guigó R, Hubbard TJ, Kent WJ, Lieb JD, Margulies
922 EH, Myers RM, Stamatoyannopoulos JA, Tenenbaum SA, Weng Z, White KP, Wold B, Yu Y, Wrobel J,
923 Risk BA, Gunawardena HP, Kuiper HC, Maier CW, Xie L, Chen X, Mikkelsen TS, Gillespie S, Goren A,
924 Ram O, Zhang X, Wang L, Issner R, Coyne MJ, Durham T, Ku M, Truong T, Eaton ML, Dobin A, Tanzer
925 A, Lagarde J, Lin W, Xue C, Williams BA, Zaleski C, Röder M, Kokocinski F, Abdelhamid RF, Alioto T,
926 Antoshechkin I, Baer MT, Batut P, Bell I, Bell K, Chakrabortty S, Chrast J, Curado J, Derrien T,
927 Drenkow J, Dumais E, Dumais J, Duttagupta R, Fastuca M, Fejes-Toth K, Ferreira P, Foissac S,
928 Fullwood MJ, Gao H, Gonzalez D, Gordon A, Howald C, Jha S, Johnson R, Kapranov P, King B,
929 Kingswood C, Li G, Luo OJ, Park E, Preall JB, Presaud K, Ribeca P, Robyr D, Ruan X, Sammeth M,

930 Sandhu KS, Schaeffer L, See LH, Shahab A, Skancke J, Suzuki AM, Takahashi H, Tilgner H, Trout D,
931 Walters N, Wang H, Hayashizaki Y, Reymond A, Antonarakis SE, Hannon GJ, Ruan Y, Carninci P,
932 Sloan CA, Learned K, Malladi VS, Wong MC, Barber GP, Cline MS, Dreszer TR, Heitner SG, Karolchik
933 D, Kirkup VM, Meyer LR, Long JC, Maddren M, Raney BJ, Grasfeder LL, Giresi PG, Battenhouse A,
934 Sheffield NC, Showers KA, London D, Bhinge AA, Shestak C, Schaner MR, Kim SK, Zhang ZZ,
935 Mieczkowski PA, Mieczkowska JO, Liu Z, McDaniell RM, Ni Y, Rashid NU, Kim MJ, Adar S, Zhang
936 Zhancheng, Wang T, Winter D, Keefe D, Iyer VR, Zheng M, Wang P, Gertz J, Vielmetter J, Partridge
937 EC, Varley KE, Gasper C, Bansal A, Pepke S, Jain P, Amrhein H, Bowling KM, Anaya M, Cross MK,
938 Muratet MA, Newberry KM, McCue K, Nesmith AS, Fisher-Aylor KI, Pusey B, DeSalvo G, Parker SL,
939 Balasubramanian Sreeram, Davis NS, Meadows SK, Eggleston T, Newberry JS, Levy SE, Absher DM,
940 Wong WH, Blow MJ, Visel A, Pennachio LA, Petrykowska HM, Abyzov A, Aken B, Barrell D, Barson
941 G, Berry A, Bignell A, Boychenko V, Bussotti G, Davidson C, Despacio-Reyes G, Diekhans M, Ezkurdia
942 I, Frankish A, Gilbert J, Gonzalez JM, Griffiths E, Harte R, Hendrix DA, Hunt T, Jungreis I, Kay M,
943 Khurana E, Leng J, Lin MF, Loveland J, Lu Z, Manthravadi D, Mariotti M, Mudge J, Mukherjee G,
944 Notredame C, Pei B, Rodriguez JM, Saunders G, Sboner A, Searle S, Sisu C, Snow C, Steward C,
945 Tapanari E, Tress ML, Van Baren MJ, Washietl S, Wilming L, Zadissa A, Zhang Zhengdong, Brent M,
946 Haussler D, Valencia A, Addleman N, Alexander RP, Auerbach RK, Balasubramanian Suganthi,
947 Bettinger K, Bhardwaj N, Boyle AP, Cao AR, Cayting P, Charos A, Cheng Y, Eastman C, Euskirchen G,
948 Fleming JD, Grubert F, Habegger L, Hariharan M, Harmanci A, Iyengar S, Jin VX, Karczewski KJ,
949 Kasowski M, Lacroute P, Lam H, Lamarre-Vincent N, Lian J, Lindahl-Allen M, Min R, Miotto B,
950 Monahan H, Moqtaderi Z, Mu XJ, O'Geen H, Ouyang Z, Patacsil D, Raha D, Ramirez L, Reed B, Shi M,
951 Slifer T, Witt H, Wu L, Xu X, Yan KK, Yang X, Struhl K, Weissman SM, Penalva LO, Karmakar S,
952 Bhanvadia RR, Choudhury A, Domanus M, Ma L, Moran J, Victorsen A, Auer T, Centanin L,
953 Eichenlaub M, Gruhl F, Heermann S, Hoeckendorf B, Inoue D, Kellner T, Kirchmaier S, Mueller C,

954 Reinhardt R, Schertel L, Schneider S, Sinn R, Wittbrodt B, Wittbrodt J, Jain G, Balasundaram G,
955 Bates DL, Byron R, Canfield TK, Diegel MJ, Dunn D, Ebersol AK, Frum T, Garg K, Gist E, Hansen RS,
956 Boatman L, Haugen E, Humbert R, Johnson AK, Johnson EM, Kutyavin T V., Lee K, Lotakis D,
957 Maurano MT, Neph SJ, Neri F V., Nguyen ED, Qu H, Reynolds AP, Roach V, Rynes E, Sanchez ME,
958 Sandstrom RS, Shafer AO, Stergachis AB, Thomas S, Vernot B, Vierstra J, Vong S, Wang Hao,
959 Weaver MA, Yan Y, Zhang M, Akey JM, Bender M, Dorschner MO, Groudine M, MacCoss MJ, Navas
960 P, Stamatoyannopoulos G, Beal K, Brazma A, Flicek P, Johnson N, Lukk M, Luscombe NM, Sobral D,
961 Vaquerizas JM, Batzoglou S, Sidow A, Hussami N, Kyriazopoulou-Panagiotopoulou S, Libbrecht MW,
962 Schaub MA, Miller W, Bickel PJ, Banfai B, Boley NP, Huang H, Li JJ, Noble WS, Bilmes JA, Buske OJ,
963 Sahu AD, Kharchenko P V., Park PJ, Baker D, Taylor J, Lochovsky L. 2012. An integrated
964 encyclopedia of DNA elements in the human genome. *Nature* **489**:57–74.
965 doi:10.1038/NATURE11247

966 Filardo EJ, Quinn JA, Raymond Frackelton A, Bland KI. 2002. Estrogen action via the G protein-coupled
967 receptor, GPR30: stimulation of adenylyl cyclase and cAMP-mediated attenuation of the epidermal
968 growth factor receptor-to-MAPK signaling axis. *Mol Endocrinol* **16**:70–84.
969 doi:10.1210/MEND.16.1.0758

970 Gassner FX, Reifenstein ECJ, Algeo JW, Mattox WE. 1958. Effects of hormones on growth, fattening, and
971 meat production potential of livestock - PubMed. *Recent Prog Horm Res* **14**:183–210; discussion
972 210-7.

973 Goodman M, Mandel JS, Desesso JM, Scialli AR. 2014. Atrazine and pregnancy outcomes: A systematic
974 review of epidemiologic evidence. *Birth Defects Res Part B - Dev Reprod Toxicol*.
975 doi:10.1002/bdrb.21101

976 Gpr107 (G protein-coupled receptor 107) - Rat Genome Database. n.d.

https://rgd.mcw.edu/rgdweb/report/gene/main.html?id=1305882

Gpr161 (G protein-coupled receptor 161) - Rat Genome Database. n.d. https://rgd.mcw.edu/rgdweb/report/gene/main.html?id=1563245

Gpr89b (G protein-coupled receptor 89B) - Rat Genome Database. n.d. https://rgd.mcw.edu/rgdweb/report/gene/main.html?id=1304837

Gprc5a (G protein-coupled receptor, class C, group 5, member A) - Rat Genome Database. n.d. https://rgd.mcw.edu/rgdweb/report/gene/main.html?id=1310804

Gprc5b (G protein-coupled receptor, class C, group 5, member B) - Rat Genome Database. n.d. https://rgd.mcw.edu/rgdweb/report/gene/main.html?id=1309510

Guerrero-Bosagna C, Covert TR, Haque MM, Settles M, Nilsson EE, Anway MD, Skinner MK. 2012. Epigenetic transgenerational inheritance of vinclozolin induced mouse adult onset disease and associated sperm epigenome biomarkers. *Reprod Toxicol* **34**:694–707. doi:10.1016/j.reprotox.2012.09.005

Hajkova P. 2011. Epigenetic reprogramming in the germline: Towards the ground state of the epigenome. *Philos Trans R Soc B Biol Sci*. doi:10.1098/rstb.2011.0042

Hansen KD, Langmead B, Irizarry RA. 2012. BSmooth: from whole genome bisulfite sequencing reads to differentially methylated regions. doi:10.1186/gb-2012-13-10-R83

Hao Z, Lv D, Ge Y, Shi J, Dolf W, Yu G, Chen J. 2020. RIdeogram: Drawing SVG Graphics to Visualize and Map Genome-Wide Data on Idiograms.

Hayashi K, Ohta H, Kurimoto K, Aramaki S, Saitou M. 2011. Reconstitution of the mouse germ cell specification pathway in culture by pluripotent stem cells. *Cell* **146**:519–532.

998 doi:10.1016/j.cell.2011.06.052

999 Henley D V, Korach KS. 2010. Physiological effects and mechanisms of action of endocrine disrupting
1000 chemicals that alter estrogen signaling. *Hormones* **9**:191–205. doi:10.14310/horm.2002.1270

1001 Hochedlinger K, Yamada Y, Beard C, Jaenisch R. 2005. Ectopic Expression of Oct-4 Blocks Progenitor-Cell
1002 Differentiation and Causes Dysplasia in Epithelial Tissues. *Cell* **121**:465–477.
1003 doi:10.1016/J.CELL.2005.02.018

1004 Huang W, Zhao C, Zhong H, Zhang S, Xia Y, Cai Z. 2019. Bisphenol S induced epigenetic and
1005 transcriptional changes in human breast cancer cell line MCF-7. *Environ Pollut* **246**:697–703.
1006 doi:10.1016/j.envpol.2018.12.084

1007 Ishikura Y, Yabuta Y, Ohta H, Hayashi K, Nakamura T, Okamoto I, Yamamoto T, Kurimoto K, Shirane K,
1008 Sasaki H, Saitou M. 2016. In Vitro Derivation and Propagation of Spermatogonial Stem Cell Activity
1009 from Mouse Pluripotent Stem Cells. *Cell Rep* **17**:2789–2804.

1010 Jühling F, Kretzmer H, Bernhart SH, Otto C, Stadler PF, Hoffmann S. 2016. metilene: fast and sensitive
1011 calling of differentially methylated regions from bisulfite sequencing data. *Genome Res* **26**:256.
1012 doi:10.1101/GR.196394.115

1013 Kabir ER, Rahman MS, Rahman I. 2015. A review on endocrine disruptors and their possible impacts on
1014 human health. *Environ Toxicol Pharmacol*. doi:10.1016/j.etap.2015.06.009

1015 Karaman EF, Ozden S. 2019. Alterations in global DNA methylation and metabolism-related genes
1016 caused by zearalenone in MCF7 and MCF10F cells. *Mycotoxin Res* **35**:309–20. doi:10.1007/s12550-
1017 019-00358-8

1018 Karl AF, Griswold MD. 1990. Sertoli cells of the testis: preparation of cell cultures and effects of
1019 retinoids. *Methods Enzymol* **190**:71–75. doi:10.1016/0076-6879(90)90010-X

1020 Kelce, William R, Stone, Christy R, Laws, Susan C, Gray, Earl. 1995. Persistent DDT metabolite p,p'-DDE is
1021 a potent androgen receptor antagonist. *Nature* **375**:6532–581.

1022 King DJ, Freimanis G, Lasecka-Dykes L, Asfor A, Ribeca P, Waters R, King DP, Laing E. 2020. A Systematic
1023 Evaluation of High-Throughput Sequencing Approaches to Identify Low-Frequency Single
1024 Nucleotide Variants in Viral Populations. *Viruses* **12**. doi:10.3390/V12101187

1025 Kurimoto K, Saitou M. 2018. Epigenome regulation during germ cell specification and development from
1026 pluripotent stem cells. *Curr Opin Genet Dev* **52**:57–64. doi:10.1016/J.GDE.2018.06.004

1027 Lau KYC, Rubinstein H, Gantner CW, Hadas R, Amadei G, Stelzer Y, Zernicka-Goetz M. 2022. Mouse
1028 embryo model derived exclusively from embryonic stem cells undergoes neurulation and heart
1029 development. *Cell Stem Cell* **29**:1445-1458.e8. doi:10.1016/J.STEM.2022.08.013

1030 Lawrence M, Gentleman R, Carey V. 2009. rtracklayer: an R package for interfacing with genome
1031 browsers. *Bioinformatics* **25**:1841–1842. doi:10.1093/BIOINFORMATICS/BTP328

1032 Lawrence M, Huber W, Pagès H, Aboyoun P, Carlson M, Gentleman R, Morgan MT, Carey VJ. 2013.
1033 Software for Computing and Annotating Genomic Ranges. *PLOS Comput Biol* **9**:e1003118.
1034 doi:10.1371/JOURNAL.PCBI.1003118

1035 Lee HJ, Hore TA, Reik W. 2014. Reprogramming the methylome: erasing memory and creating diversity.
1036 *Cell Stem Cell* **14**:710–9. doi:10.1016/j.stem.2014.05.008

1037 Lee S, Cook D, Lawrence M. 2019. Plyranges: A grammar of genomic data transformation. *Genome Biol*
1038 **20**:1–10. doi:10.1186/S13059-018-1597-8/FIGURES/5

1039 Lehle JD, McCarrey JR. 2023. Accelerating the alignment processing speed of the comprehensive end-to-
1040 end whole-genome bisulfite sequencing pipeline, wg-blimp. *Biol Methods Protoc* **8**.
1041 doi:10.1093/BIOMETHODS/BPAD012

1042 Liao Y, Smyth GK, Shi W. 2019. The R package Rsubread is easier, faster, cheaper and better for
1043 alignment and quantification of RNA sequencing reads. *Nucleic Acids Res* **47**.
1044 doi:10.1093/NAR/GKZ114

1045 Mason CE, Shu FJ, Wang C, Session RM, Kallen RG, Sidell N, Yu T, Liu MH, Cheung E, Kallen CB. 2010.
1046 Location analysis for the estrogen receptor-α reveals binding to diverse ERE sequences and
1047 widespread binding within repetitive DNA elements. *Nucleic Acids Res* **38**:2355.
1048 doi:10.1093/NAR/GKP1188

1049 McCarthy DJ, Chen Y, Smyth GK. 2012. Differential expression analysis of multifactor RNA-Seq
1050 experiments with respect to biological variation. *Nucleic Acids Res* **40**:4288–4297.
1051 doi:10.1093/NAR/GKS042

1052 Meccariello R, Chianese R, Chioccarelli T, Ciaramella V, Fasano S, Pierantoni R, Cobellis G. 2014. Intra-
1053 testicular signals regulate germ cell progression and production of qualitatively mature
1054 spermatozoa in vertebrates. *Front Endocrinol (Lausanne)*. doi:10.3389/fendo.2014.00069

1055 Merkel A, Fernández-Callejo M, Casals E, Marco-Sola S, Schuyler R, Gut IG, Heath SC. 2019. gemBS: high
1056 throughput processing for DNA methylation data from bisulfite sequencing. *Bioinformatics* **35**:737–
1057 742. doi:10.1093/BIOINFORMATICS/BTY690

1058 Molina L, Figueroa CD, Bhoola KD, Ehrenfeld P. 2017. GPER-1/GPR30 a novel estrogen receptor sited in
1059 the cell membrane: therapeutic coupling to breast cancer. *Expert Opin Ther Targets* **21**:755–766.
1060 doi:10.1080/14728222.2017.1350264

1061 Monti M, Redi CA. 2016. Isolation and Characterization of Mouse Antral Oocytes Based on Nucleolar
1062 Chromatin Organization. *J Vis Exp* **2016**. doi:10.3791/53616

1063 Morgan M, Obenchain V, Hester J, Pagès H. 2023. SummarizedExperiment container.

1064 Myers RM, Stamatoyannopoulos J, Snyder M, Dunham I, Hardison RC, Bernstein BE, Gingeras TR, Kent
1065 WJ, Birney E, Wold B, Crawford GE, Epstein CB, Shoresh N, Ernst J, Mikkelsen TS, Kheradpour P,
1066 Zhang X, Wang L, Issner R, Coyne MJ, Durham T, Ku M, Truong T, Ward LD, Altshuler RC, Lin MF,
1067 Kellis M, Davis CA, Kapranov P, Dobin A, Zaleski C, Schlesinger F, Batut P, Chakrabortty S, Jha S, Lin
1068 W, Drenkow J, Wang Huaien, Bell K, Bell I, Gao H, Dumais E, Dumais J, Antonarakis SE, Ucla C, Borel
1069 C, Guigo R, Djebali S, Lagarde J, Kingswood C, Ribeca P, Sammeth M, Alioto T, Merkel A, Tilgner H,
1070 Carninci P, Hayashizaki Y, Lassmann T, Takahashi H, Abdelhamid RF, Hannon G, Fejes KT, Preall J,
1071 Gordon A, Sotirova V, Reymond A, Howald C, Graison EAY, Chrast J, Ruan Y, Ruan X, Shahab A, Poh
1072 WT, Wei CL, Furey TS, Boyle AP, Sheffield NC, Song L, Shibata Y, Vales T, Winter D, Zhang Z, London
1073 D, Wang Tianyuan, Keefe D, Iyer VR, Lee BK, McDaniell RM, Liu Z, Battenhouse A, Bhinge AA, Lieb
1074 JD, Grasfeder LL, Showers KA, Giresi PG, Kim SKC, Shestak C, Pauli F, Reddy TE, Gertz J, Partridge
1075 EC, Jain P, Sprouse RO, Bansal A, Pusey B, Muratet MA, Varley KE, Bowling KM, Newberry KM,
1076 Nesmith AS, Dilocker JA, Parker SL, Waite LL, Thibeault K, Roberts K, Absher DM, Mortazavi A,
1077 Williams B, Marinov G, Trout D, King B, McCue K, Kirilusha A, DeSalvo G, Fisher KA, Amrhein H,
1078 Pepke S, Vielmetter J, Sherlock G, Sidow A, Batzoglou S, Rauch R, Kundaje A, Libbrecht M,
1079 Margulies EH, Parker SCJ, Elnitski L, Green ED, Hubbard T, Harrow J, Searle S, Parker SCJ, Aken B,
1080 Frankish A, Hunt T, Despacio-Reyes G, Kay M, Mukherjee G, Bignell A, Saunders G, Boychenko V,
1081 Brent M, van Baren MJ, Brown RH, Gerstein M, Khurana E, Balasubramanian S, Lam H, Cayting P,
1082 Robilotto R, Lu Z, Derrien T, Tanzer A, Knowles DG, Mariotti M, Haussler D, Harte R, Diekhans M,
1083 Lin M, Valencia A, Tress M, Rodriguez JM, Raha D, Shi M, Euskirchen G, Grubert F, Kasowski M, Lian
1084 J, Lacroute P, Xu Y, Monahan H, Patacsil D, Slifer T, Yang X, Charos A, Reed B, Wu L, Auerbach RK,
1085 Habegger L, Hariharan M, Rozowsky J, Abyzov A, Weissman SM, Struhl K, Lamarre-Vincent N,
1086 Lindahl-Allen M, Miotto B, Moqtaderi Z, Fleming JD, Newburger P, Farnham PJ, Frietze S, O'Geen H,
1087 Xu X, Blahnik KR, Cao AR, Iyengar S, Kaul R, Thurman RE, Wang Hao, Navas PA, Sandstrom R, Sabo

1088 PJ, Weaver M, Canfield T, Lee K, Neph S, Roach V, Reynolds A, Johnson A, Rynes E, Giste E, Vong S,
1089 Neri J, Frum T, Nguyen ED, Ebersol AK, Sanchez ME, Sheffer HH, Lotakis D, Haugen E, Humbert R,
1090 Kutyavin T, Shafer T, Noble WS, Dekker J, Lajoie BR, Sanyal A, Rosenbloom KR, Dreszer TR, Raney
1091 BJ, Barber GP, Meyer LR, Sloan CA, Malladi VS, Cline MS, Learned K, Swing VK, Zweig AS, Rhead B,
1092 Fujita PA, Roskin K, Karolchik D, Kuhn RM, Wilder SP, Sobral D, Herrero J, Beal K, Lukk M, Brazma A,
1093 Vaquerizas JM, Luscombe NM, Bickel PJ, Boley N, Brown JB, Li Q, Huang H, Sboner A, Yip KY, Cheng
1094 C, Yan KK, Bhardwaj N, Wang Jing, Lochovsky L, Jee J, Gibson T, Leng J, Du J, Harris RS, Song G,
1095 Miller W, Suh B, Paten B, Hoffman MM, Buske OJ, Weng Z, Dong X, Wang Jie, Xi H, Tenenbaum SA,
1096 Doyle F, Chittur S, Penalva LO, Tullius TD, White KP, Karmakar S, Victorsen A, Jameel N, Bild N,
1097 Grossman RL, Collins PJ, Trinklein ND, Giddings MC, Khatun J, Maier C, Wang Ting, Whitfield TW,
1098 Chen X, Yu Y, Gunawardena H, Feingold EA, Lowdon RF, Dillon LAL, Good PJ, Risk B. 2011. A user's
1099 guide to the encyclopedia of DNA elements (ENCODE). *PLoS Biol* **9**.
1100 doi:10.1371/JOURNAL.PBIO.1001046

1101 Neuwirth E. 2022. RColorBrewer: ColorBrewer Palettes.

1102 Nilsson EE, Anway MD, Stanfield J, Skinner MK. 2008. Transgenerational epigenetic effects of the
1103 endocrine disruptor vinclozolin on pregnancies and female adult onset disease. *Reproduction*
1104 **135**:713–721. doi:10.1530/REP-07-0542

1105 Nystrom S. 2023. motif matching, comparison, and de novo discovery using the MEME Suite.

1106 Ohta H, Kurimoto K, Okamoto I, Nakamura T, Yabuta Y, Miyauchi H, Yamamoto T, Okuno Y, Hagiwara M,
1107 Shirane K, Sasaki H, Saitou M. 2017. In vitro expansion of mouse primordial germ cell- like cells
1108 recapitulates an epigenetic blank slate. *EMBO J* **36**:1888–1907. doi:10.15252/embj

1109 Okonechnikov K, Conesa A, García-Alcalde F. 2016. Qualimap 2: advanced multi-sample quality control
1110 for high-throughput sequencing data. *Bioinformatics* **32**:292–294.

1111 doi:10.1093/BIOINFORMATICS/BTV566

1112 Ozgyin L, Erdos E, Bojcsuk D, Balint BL. 2015. Nuclear receptors in transgenerational epigenetic
1113 inheritance. *Prog Biophys Mol Biol*. doi:10.1016/j.pbiomolbio.2015.02.012

1114 Pagès H, Carlson M, Falcon S, Li N. 2023. AnnotationDbi: Manipulation of SQLite-based annotations in
1115 Bioconductor. doi:10.18129/B9.bioc.AnnotationDbi

1116 Patrat C, Okamoto I, Diabangouaya P, Vialon V, Le Baccon P, Chow J, Heard E. 2009. Dynamic changes in
1117 paternal X-chromosome activity during imprinted X-chromosome inactivation in mice. *Proc Natl*
1118 *Acad Sci U S A* **106**:5198–5203. doi:10.1073/pnas.0810683106

1119 Picard Tools - By Broad Institute. n.d. https://broadinstitute.github.io/picard/

1120 Ribeiro E, Delgadinho M, Brito M. 2019. Environmentally Relevant Concentrations of Bisphenol A
1121 Interact with Doxorubicin Transcriptional Effects in Human Cell Lines. *Toxics* **7**.
1122 doi:10.3390/TOXICS7030043

1123 Rio DC, Ares M, Hannon GJ, Nilsen TW. 2010. Purification of RNA using TRIzol (TRI Reagent). *Cold Spring*
1124 *Harb Protoc* **5**:1–4. doi:10.1101/pdb.prot5439

1125 Robinson MD, McCarthy DJ, Smyth GK. 2010. edgeR: a Bioconductor package for differential expression
1126 analysis of digital gene expression data. *Bioinformatics* **26**:139–140.
1127 doi:10.1093/BIOINFORMATICS/BTP616

1128 Robinson MD, Oshlack A. 2010. A scaling normalization method for differential expression analysis of
1129 RNA-seq data. *Genome Biol* **11**:1–9. doi:10.1186/GB-2010-11-3-R25/FIGURES/3

1130 Rodig SJ. 2022. Cell Staining. *Cold Spring Harb Protoc* **2022**:pdb.top099606. doi:10.1101/PDB.TOP099606

1131 Roy SK, Greenwald GS. 1996. Methods of separation and in-vitro culture of pre-antral follicles from

1132 mammalian ovaries. *Hum Reprod Update* **2**:236–245.

1133 Ryan D. n.d. MethylDackel: A (mostly) universal methylation extractor for BS-seq experiments.
1134 https://github.com/dpryan79/MethylDackel

1135 Sambrook J, Russell DW. 2006. Purification of Nucleic Acids by Extraction with Phenol:Chloroform. *Cold*
1136 *Spring Harb Protoc* **2006**. doi:10.1101/PDB.PROT4455

1137 Santos F, Hendrich B, Reik W, Dean W. 2002. Dynamic Reprogramming of DNA Methylation in the Early
1138 Mouse Embryo. *Dev Biol* **241**:172–82. doi:10.1006/dbio.2001.0501

1139 Sanz LA, Kota SK, Feil R. 2010. Genome-wide DNA demethylation in mammals. *Genome Biol* **11**.
1140 doi:10.1186/gb-2010-11-3-110

1141 Schilbert HM, Rempel A, Pucker B. 2020. Comparison of Read Mapping and Variant Calling Tools for the
1142 Analysis of Plant NGS Data. *Plants 2020, Vol 9, Page 439* **9**:439. doi:10.3390/PLANTS9040439

1143 Schindelin J, Arganda-Carreras I, Frise E, Kaynig V, Longair M, Pietzsch T, Preibisch S, Rueden C, Saalfeld
1144 S, Schmid B, Tinevez JY, White DJ, Hartenstein V, Eliceiri K, Tomancak P, Cardona A. 2012. Fiji: an
1145 open-source platform for biological-image analysis. *Nat Methods 2012 97* **9**:676–682.
1146 doi:10.1038/nmeth.2019

1147 Senyildiz M, Karaman EF, Bas SS, Pirincci PA, Ozden S. 2017. Effects of BPA on global DNA methylation
1148 and global histone 3 lysine modifications in SH-SY5Y cells: An epigenetic mechanism linking the
1149 regulation of chromatin modifiying genes. *Toxicol Vitr* **44**:313–321. doi:10.1016/j.tiv.2017.07.028

1150 Sloan CA, Chan ET, Davidson JM, Malladi VS, Strattan JS, Hitz BC, Gabdank I, Narayanan AK, Ho M, Lee
1151 BT, Rowe LD, Dreszer TR, Roe G, Podduturi NR, Tanaka F, Hong EL, Cherry JM. 2016. ENCODE data
1152 at the ENCODE portal. *Nucleic Acids Res* **44**:D726–D732. doi:10.1093/NAR/GKV1160

1153 Slowikowski K, Schep A, Hughes S, Dang TK, Lukauskas S, Irisson J-O, Kamvar ZN, Ryan T, Christophe D,
1154 Hiroaki Y, Gramme P, Abdol AM, Barrett M, Cannoodt R, Krassowski M, Chirico M, Aphalo P. 2023.
1155 ggrepel: Automatically Position Non-Overlapping Text Labels with "ggplot2."

1156 Smith AD, de Sena Brandine G. 2021. Falco: High-speed FastQC emulation for quality control of
1157 sequencing data. *F1000Research* **8**. doi:10.12688/F1000RESEARCH.21142.2/DOI

1158 Song A, Ona J, Osuna C, Phandthong R, Talbot P. 2023. Establishing a Disease-in-a-Dish Model to Study
1159 SARS-CoV-2 Infection During Prenatal Development. *Curr Protoc* **3**. doi:10.1002/CPZ1.759

1160 Song K-H, Lee K, Choi H-S. 2011. Endocrine Disrupter Bisphenol A Induces Orphan Nuclear Receptor
1161 Nur77 Gene Expression and Steroidogenesis in Mouse Testicular Leydig Cells. *Endocrinology*
1162 **143**:2208–2215. doi:10.1210/endo.143.6.8847

1163 Swedenborg E, Rüegg J, Mäkelä S, Pongratz I. 2009. Endocrine disruptive chemicals: mechanisms of
1164 action and involvement in metabolic disorders. *J Mol Endocrinol* **43**:1–10. doi:10.1677/jme-08-
1165 0132

1166 Team BC. 2015. Mus.musculus: Annotation package for the Mus.musculus object.
1167 doi:10.18129/B9.bioc.Mus.musculus

1168 Team TBD. 2021. BSgenome.Mmusculus.UCSC.mm10: Full genome sequences for Mus musculus (UCSC
1169 version mm10, based on GRCm38.p6). doi:10.18129/B9.bioc.BSgenome.Mmusculus.UCSC.mm10

1170 Thomas P, Dong J. 2006. Binding and activation of the seven-transmembrane estrogen receptor GPR30
1171 by environmental estrogens: A potential novel mechanism of endocrine disruption. *J Steroid*
1172 *Biochem Mol Biol* **102**:175–179. doi:10.1016/j.jsbmb.2006.09.017

1173 Tremblay B. 2023. universalmotif: Import, Modify, and Export Motifs with R.

1174 Triche TJ, Weisenberger DJ, Van Den Berg D, Laird PW, Siegmund KD. 2013. Low-level processing of
1175 Illumina Infinium DNA Methylation BeadArrays. *Nucleic Acids Res* **41**:e90–e90.
1176 doi:10.1093/NAR/GKT090

1177 vom Saal FS, Hughes C. 2005. An extensive new literature concerning low-dose effects of bisphenol A
1178 shows the need for a new risk assessment. *Environ Health Perspect*. doi:10.1289/ehp.7713

1179 Wang J, Zhuang J, Iyer S, Lin XY, Greven MC, Kim BH, Moore J, Pierce BG, Dong X, Virgil D, Birney E, Hung
1180 JH, Weng Z. 2013. Factorbook.org: a Wiki-based database for transcription factor-binding data
1181 generated by the ENCODE consortium. *Nucleic Acids Res* **41**:D171–D176.
1182 doi:10.1093/NAR/GKS1221

1183 Wang J, Zhuang J, Iyer S, Lin XY, Whitfield TW, Greven MC, Pierce BG, Dong X, Kundaje A, Cheng Y,
1184 Rando OJ, Birney E, Myers RM, Noble WS, Snyder M, Weng Z. 2012. Sequence features and
1185 chromatin structure around the genomic regions bound by 119 human transcription factors.
1186 *Genome Res* **22**:1798–1812. doi:10.1101/GR.139105.112

1187 Wang T, Pehrsson EC, Purushotham D, Li D, Zhuo X, Zhang B, Lawson HA, Province MA, Krapp C, Lan Y,
1188 Coarfa C, Katz TA, Tang WY, Wang Z, Biswal S, Rajagopalan S, Colacino JA, Tsai ZTY, Sartor MA,
1189 Neier K, Dolinoy DC, Pinto J, Hamanaka RB, Mutlu GM, Patisaul HB, Aylor DL, Crawford GE,
1190 Wiltshire T, Chadwick LH, Duncan CG, Garton AE, McAllister KA, Bartolomei MS, Walker CL, Tyson
1191 FL. 2018. The NIEHS TaRGET II Consortium and environmental epigenomics. *Nat Biotechnol*.
1192 doi:10.1038/nbt.4099

1193 Wickham H, Chang W, Henry L, Pedersen TL, Takahashi K, Wilke C, Woo K, Yutani H, Dunnington D, Posit
1194 P. 2023a. ggplot2: Create Elegant Data Visualisations Using the Grammar of Graphics.

1195 Wickham H, François R, Henry L, Müller K, Vaughan D, Posit Software P. 2023b. dplyr: A Grammar of

Data Manipulation.

Wickham H, RStudio. 2022. stringr: Simple, Consistent Wrappers for Common String Operations.

Wickham H, Vaughan D, Girlich M, Ushey K, Posit Software, PBC. 2023c. tidyr: Tidy Messy Data.

Wöste M, Leitão E, Laurentino S, Horsthemke B, Rahmann S, Schröder C. 2020. Wg-blimp: An end-to-end analysis pipeline for whole genome bisulfite sequencing data. *BMC Bioinformatics* **21**:1–8. doi:10.1186/S12859-020-3470-5/FIGURES/3

Wright K. 2023. pals: Color Palettes, Colormaps, and Tools to Evaluate Them.

Xie Y, Sarma A, Vogt A, Andrew A, Zvoleff A, Al-Zubaidi A, Simon A, Atkins A, Baumer W, Wolen A, Manton A, Yasumoto A, Baumer B, Diggs B, Zhang B, Yapparov B, Pereira C, Dervieux C, Hall D, Hugh-Jones D, Robinson D, Hemken D, Murdoch D, Campitelli E, Hughes E, Riederer E, Hirschmann F, Simeon F, Fang F, Jr FEH, Aden-Buie G, Detrez G, Wickham H, Zhu H, Jeon H, Bengtsson H, Yutani H, Lyttle I, Daniel H, Bien J, Burkhead J, Manton J, Lander J, Punyon J, Luraschi J, Arnold J, Bryan J, Ashkenas J, Stephens J, Hester J, Cheng J, Ranke J, Honaker J, Muschelli J, Keane J, Allaire J, Toloe J, Sidi J, Larmarange J, Barnier J, Zhong K, Slowikowski K, Forner K, Smith KK, Mueller K, Takahashi K, Walthert L, Gallindo L, Hofert M, Modrák M, Chirico M, Friendly M, Bojanowski M, Kuhlmann M, Patrick M, Caballero N, Salkowski N, Hansen NR, Ross N, Mahdi O, Krivitsky PN, Faria P, Li Q, Vaidyanathan R, Cotton R, Krzyzanowski R, Copetti R, Francois R, Williamson R, Mati S, Kostyshak S, Meyer S, Brouwer S, Bernard S de, Rousseau S, Wei T, Assus T, Lamadon T, Leeper T, Mastny T, Torsney-Weir T, Davis T, Veitas V, Zhu W, Wu W, Foster Z, Kamvar ZN, Posit Software P. 2023. knitr: A General-Purpose Package for Dynamic Report Generation in R.

Yan L. 2023. ggvenn: Draw Venn Diagram by “ggplot2.”

Ye J, Coulouris G, Zaretskaya I, Cutcutache I, Rozen S, Madden TL. 2012. Primer-BLAST: a tool to design

1218 target-specific primers for polymerase chain reaction. *BMC Bioinformatics* **13**:134.
1219 doi:10.1186/1471-2105-13-134

1220 You L, Casanova M, Archibeque-Engle S, Sar M, Fan LQ, Heck H d'A. 1998. Impaired male sexual
1221 development in perinatal Sprague-Dawley and Long- Evans hooded rats exposed in utero and
1222 lactationally to p,p'-DDE. *Toxicol Sci* **45**:162–173. doi:10.1006/toxs.1998.2515

1223 Zhou W. 2022. wheatmap: Incrementally Build Complex Plots using Natural Semantics.

1224 Zhou W, Hinoue T, Barnes B, Mitchell O, Iqbal W, Lee SM, Foy KK, Lee KH, Moyer EJ, VanderArk A,
1225 Koeman JM, Ding W, Kalkat M, Spix NJ, Eagleson B, Pospisilik JA, Szabó PE, Bartolomei MS, Vander
1226 Schaaf NA, Kang L, Wiseman AK, Jones PA, Krawczyk CM, Adams M, Porecha R, Chen BH, Shen H,
1227 Laird PW. 2022. DNA methylation dynamics and dysregulation delineated by high-throughput
1228 profiling in the mouse. *Cell genomics* **2**. doi:10.1016/J.XGEN.2022.100144

1229 Zhou W, Triche TJ, Laird PW, Shen H. 2018. SeSAMe: reducing artifactual detection of DNA methylation
1230 by Infinium BeadChips in genomic deletions. *Nucleic Acids Res* **46**:e123–e123.
1231 doi:10.1093/NAR/GKY691

1232

1233

1234

1235

1236

1237

1238

1239 **SUPPLEMENTAL FILES**

1240

1241 **Supplementary file 1a.**

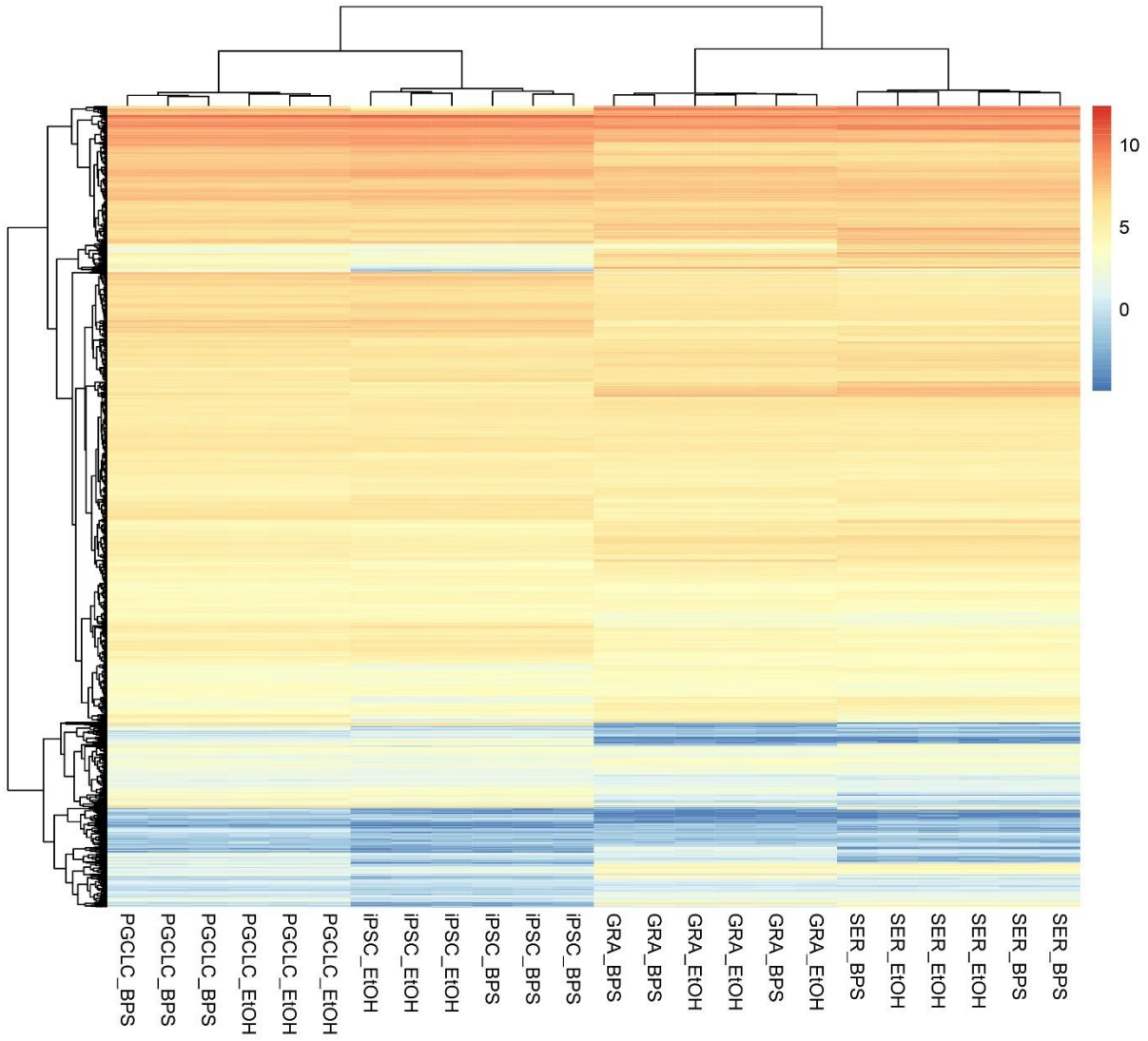

1242

1243 **Supplement figure 1. Differential expression of potential endocrine-signaling independent DMCs.**
1244 Heatmap displaying the relative expression of genes with promoters enriched for apparent endocrine-
1245 signaling independent DMCs. The majority of these genes are actively expressed in all cell types and an
1246 overall largely similar pattern of expression across all cell types.

1247

Supplementary file 1b.

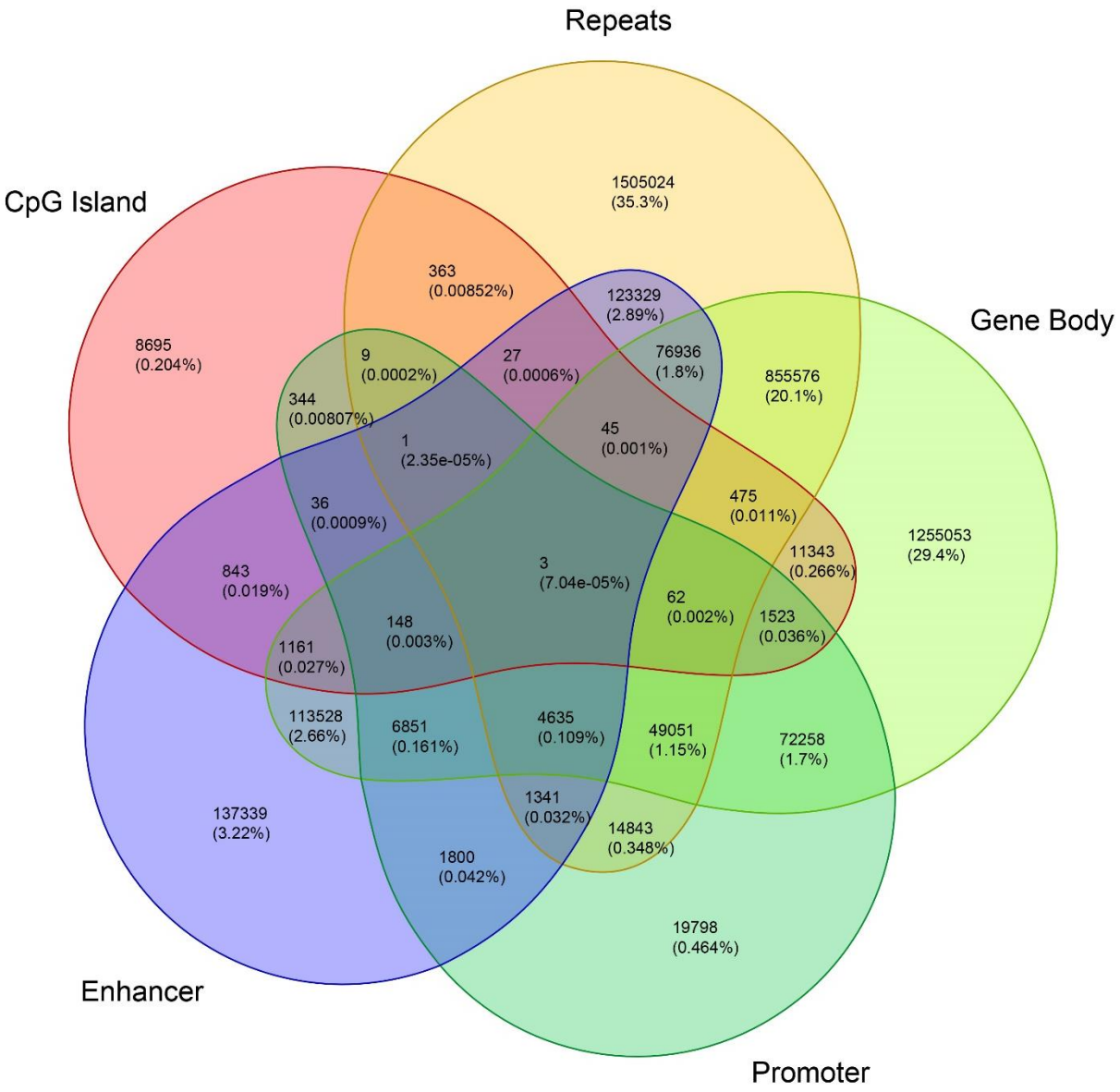

Supplement figure 2. Genome-wide annotation of ERE half-sites. Venn diagram displaying the identification of ERE half-sites localized in known genic and intergenic regions.

Supplement table 1. Summary of ERE annotations

CpG Islands	Repeat Regions	Gene Bodies	Promoters	Enhancers
25,079	2,631,743	2,448,668	172,707	468,072

1254 **Supplementary file 1c.**

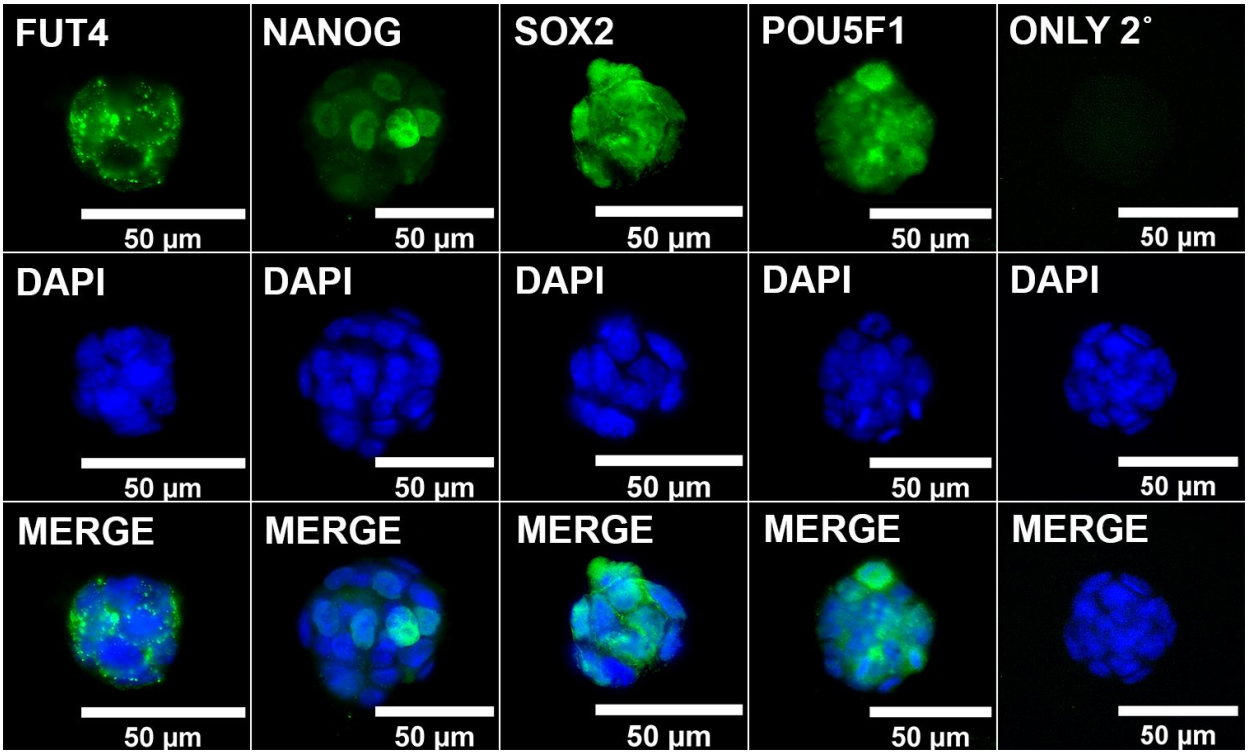

1255

1256 **Supplement figure 3. ICC validation of MF5-9-1 iPSCs.** iPSCs from reprogrammed MEFs were validated
1257 for immunolabeling with known pluripotency markers along with negative control.

1258

1259 **Supplementary file 1d.**

WiCell

Chromosome Analysis Report: 081055

Date Reported: Wednesday, April 1, 2020
Cell Line: 5-9-1
Passage#: 8
Date of Sample: 3/25/2020
Specimen: Mouse IPSC
Results: 40,XY

Cell Line Sex: Male
Reason for Testing: Study routine characterizaton
Investigator: Yu-Huey Lin, UT San Antonio

Nonclonal findings: 40,XY,Del(4C5) 41,XY,+11

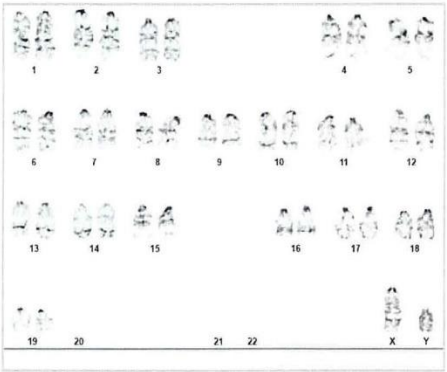

Cell: 73
Slide: G03
Slide Type: Karyotype

Total Counted: 20
Total Analyzed: 16
Total Karyogrammed: 15
Band Resolution: >230

Interpretation:
This is a normal karyotype; no clonal abnormalities were detected at the stated band level of resolution.

There are nonclonal findings, listed above, one of which contains a chromosomal aberration (gain of chromosome 11) recurrently acquired in pluripotent stem cell cultures. Nonclonal findings may result from technical artifact, but may be due to a developing clonal abnormality or to low-level mosaicism.

Completed by: Kim Leonhard, CG(ASCP)
Reviewed and Interpreted by: Kaitlin C. Lenhart, Ph.D.

Date:_____ Sent By:____ Sent To:_____ QC Review By: ____

Limitations: This assay allows for microscopic visualization of numerical and structural chromosome abnormalities. The size of structural abnormality that can be detected is >3-10Mb, dependent upon the G-band resolution obtained from this specimen. For the purposes of this report, band level is defined as the number of G-bands per haploid genome. It is documented here as "band level", i.e., the range of bands determined from the four karyograms in this assay. Detection of heterogeneity of clonal cell populations in this specimen (i.e.,mosaicism) is limited by the number of metaphase cells examined, documented here as "# of cells counted".

This assay was conducted solely for listed investigator/institution. The results of this assay are for research use only. Unless otherwise mutually agreed in writing, the services provided to you hereunder by WiCell Research Institute, Inc. ("WiCell") are governed solely by WiCell's Terms and Conditions of Service, found at www.wicell.org/privacyandterms. Any terms you may attach to a purchase order or other document that are inconsistent, add to, or conflict with WiCell's Terms and Conditions of Service are null and void and of no legal force or effect.

1260

1261 **Supplementary file 1e.**

1262 **iPSC, EpiLC, and PGCLC Media Components**

1263 Stock solutions to prepare before making media.

1264 1. Insulin stock sol. (25 mg/mL), (Sigma I-1882):

1265 100 mg in 4 mL (0.01 M HCl), overnight at 4C

1266 aliquot 0.5 mL (total 8 tubes) → -20°C

1267

1268 2. Apotransferrin stock sol. (100 mg/mL), (Sigma T-1147):

1269 500 mg in 5 mL (water), overnight at 4 C

1270 aliquot 0.5 mL (10 tubes) → -20°C

1271

1272 3. Progesterone stock sol. (0.6 mg/mL) (Sigma P8783):

1273 10 mg in 1 mL ethanol (10 mg/mL)

1274 → 60 µL of stock (10 mg/mL) + 940 µL ethanol → filter through a 0.22 µm filter

1275 aliquot 100 µL (10 tubes) → -20°C

1276

1277 4. Putrescine stock sol. (160 mg/mL) (Sigma P5780):

1278 320 mg in 2 mL water → 0.22 filter

1279 aliquot 60 µL (~30 tubes) → -20°C

1280

1281 5. Sodium selenite stock sol. (3mM) (Sigma S5261, 10G, MW:172.49)

1282 300 mM: 51.88 mg in 1 mL water → 0.22 filter

1283 10 µL (300 mM stock) + 990 µL water = 3 mM

1284 aliquot 50 µL (~20 tubes) → -20°C

1285

1286 6. Activin A stock sol. (50 µg/mL) (120-14, total 10 µg/vial, need more)

1287 20 µg (2 vials) + 400 µL water → 5 µL aliquot (~40 tubes) → -20°C

1288

1289 7. bFGF stock sol. (10 µg/mL) (13256-029, 10 µg/vial)

1290 10 µg (total) in 1 mL (10 mM Tris, pH 7.6 with 0.1 % BSA)

1291 → aliquot 20 µL → -20°C

1292

1293 8. Recombinant human BMP4 stock sol. (50 ug/mL) (314-BP-010)

1294 60 ug (total) + 1200 µL (4 mM HCl with 0.1% BSA)

1295 → aliquot 105 µL (12 tubes total) → -80°C

1296

1297 9. Stem Cell Factor (SCF) stock sol. (50 ug/µL) (455-MC-010)

1298 10 ug (total) + 200 µL (PBS with 0.1% BSA)

1299 → aliquot 21 µL (10 tubes total) → -80°C

1300

1301 10. Recombinant mouse EGF stock sol. (500 ug/mL) (2028-EG-200)

1302 200 ug (total) + 400 µL (PBS with 0.1% BSA)

1303 → aliquot 10 µL (60 tubes) → -80°C

1304 **iPSC media**

1305 **N2B27 media for culturing iPSCs in feeder-free conditions**

1306 **Supplement table 2. N2 media components (5 mL)**

Name	Volume	Catalog Number	Storage Temp
DMEM/F12	3.6 mL	21041-025	(4°C)
Insulin stock sol.	0.5 mL	I-1882	(-20°C)
Apotransferrin stock sol.	0.5 mL	T-1147	(-20°C)
7.5% BSA sol.	330 µL	15260-037	(4°C)
Progesterone stock sol.	16.5 µL	P8783	(-20°C)
Putrescine stock sol.	50 µL	P5780	(-20°C)
Sodium selenite stock sol.	5 µL	S5261	(-20°C)

1307

1308 **Supplement table 3. N2B27 media components (1 L)**

Name	Volume	Catalog Number	Storage Temp
N2	5 mL	Table 1	(RT)
DMEM/F12	495 mL	21041-025	(4°C)
Neurobasal	480 mL	12348-017	(4°C)
B27 (50X)	10 mL	12587-010	(-20°C)
Pen/Strep	5 mL	15070063	(-20°C)
L-glutamine stock sol.	5 mL	35050061/Glutamax	(4°C)
β-ME stock sol., 50 mM	1.8 mL	21985-023	(4°C)

1309

1310 Make a 40 mL aliquot of N2B27 and store at -80°C.

1311

1312 **Supplement table 4. N2B27 2i-LIF media components (40 mL)**

Name	Volume	Catalog Number	Storage Temp
N2B27	40 mL	Table 2	(-80°C)
CHIR99021	12 µL	1677-5	(-80°C)
PD0325901	3.2 µL	04-0006-02	(-80°C)

ESGRO	4 µL	ESG1107	(4°C)

1313

1314 Store at 4°C for up to 2 weeks.

1315

1316 **EpiLC differentiation**

1317 Plate coating solution.

1318 1. Human plasma fibronectin (1 mg/mL, store at 4C) (1 mg/mL, FC010, 1 mg total = 1 mL),

1319

1320 Working solution: For a 12-well plate: dilute 10 µL fibronectin with 600 µL PBS to obtain 16.6 µL/mL

1321 fibronectin solution. Pipet the solution into one well of a 12-well plate, incubate for at least 1hr at 37°C

1322 and then aspirate the fibronectin solution just before plating iPSCs.

1323

1324 **Supplement table 5. N2 EpiLC differentiation (~5 mL)**

Name	Volume	Catalog Number	Storage Temp
N2B27	5 mL	Table 2	(-80°C)
Activin A stock sol.	2 µL	120-14	(-20°C)
bFGF stock sol.	6 µL	13256-029	(-20°C)
KSR	50 µL	10828-028	(-20°C)

1325

1326

1327 **PGCLC differentiation**

1328 **Supplement table 6. GK15 (10 mL)**

Name	Volume	Catalog Number	Storage Temp
GMEM	8.082 mL	11710-035	(4°C)
KSR	1.5 mL	10828-028	(-20°C)
Non-EAA	100 µL	11140-050	(4°C)
Sodium pyruvate	100 µL	11360070	(4°C)
Pen/Strep	100 µL	15070	(4°C)
L-glutamine	100 µL	35050061/Glutamax	(4°C)
β-ME, 50 mM	18 µL	21985-023	(4°C)

1329

1330 **Supplement table 7. PGCLC differentiation media (10 mL)**

Name	Volume	Catalog Number	Storage Temp
GK15	9.878 mL	Table 5	(4°C)
BMP4	100 µL	314-BP-010	(-80°C)
SCF	20 µL	455-MC-010	(-80°C)
LIF	1 µL	ESG1107	(-80°C)
EGF	1 µL	2028-EG-200	(-80°C)

1331

1332 **Supplement table 8. TrypLE wash media (75 mL)**

Name	Volume	Catalog Number	Storage Temp
7.5% BSA sol.	1 mL	15260-037	(4°C)
DMEM/F12	74 mL	21041-025	(4°C)

1333

1334

1335 **Supplementary file 1f.**

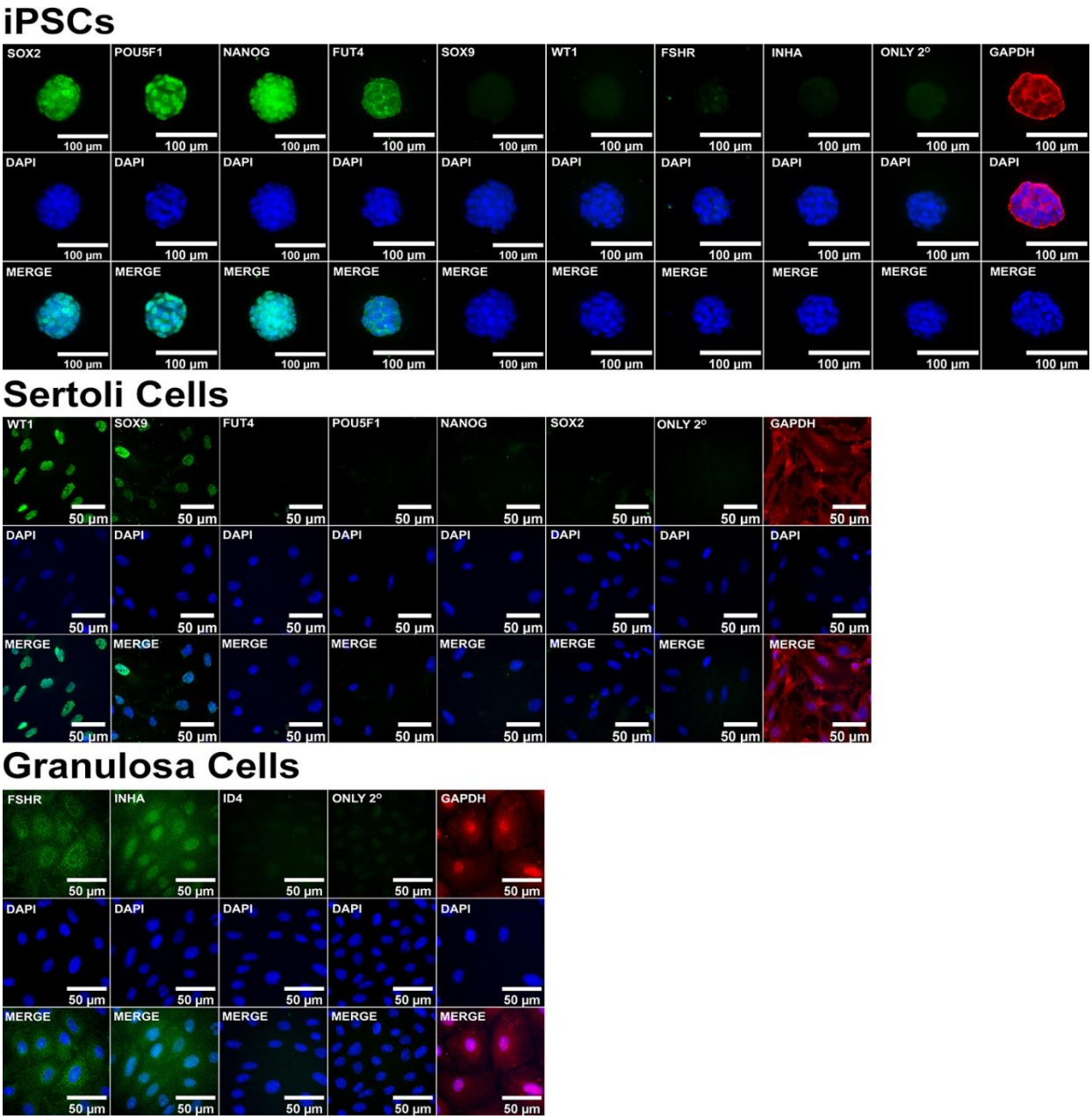

1336

1337 **Supplement figure 4. ICC control staining of cell type-specific markers.** Validation of immunolabeling
1338 for known pluripotent and somatic cell type markers in iPSCs, Sertoli Cells, and Granulosa cells along
1339 with negative and positive controls.

1340

1341

1342 **Supplementary file 1g.**

1343 **Preparation of primary cultures of Sertoli cells from mice protocol**

1344 **Materials:**

1345 500 mL DPBS (Thermo Fisher: Cat. No. 14040133)

1346 DNaseI. 6.64 mg/mL in DPBS (Sigma: Cat. No. DN-25)

1347 Trypsin 2.5% (10X Gibco) (Gibco-BRL: Cat. No. 15090-046)

1348 Soybean trypsin inhibitor, 3.4 mg/mL in DPBS (Gibco-BRL: Cat. No. 17075-011)

1349 Collagenase type IV, 0.70 mg/mL (Worthinton: Cat. No. LS004188)

1350 Sertoli cell media containing retinoic acid (ScienCell™: Cat. No. 4521)

1351 **Equipment:**

1352 Pyrex Trypsinizing Flask 300 mL Standard Flask (Fisher Cat. No. 09-552-45)

1353 **Procedure:** (maintain sterility throughout procedure)

1354 A. **Preparation of testes tissue**

1355 1. Sacrifice mice by CO_2.

1356 2. Wipe down abdomen with 70% EtOH.

1357 3. Make abdominal incision.

1358 4. Remove the testes and immerse in DPBS in a 50 mL conical tube.

1359 5. Remove tubule bundle from tunica.

1360 a. Place testes on parafilm, grasp at one end, and make a small incision in the

1361 tunica at the opposite end.

1362 b. Push the tubules out of tunica by using the side of closed scissors.

1363 c. Weigh flask with fresh DPBS (this is the DPBS volume from the first step below

1364 so you must estimate for now (W_1):_____g

1365 d. Place tubules in DPBS and weigh (W_2):_____g

1366 e. Calculate testes weight (W_T) = (W_2 - W_1):_____g.

1367

1368 B. **Preparation of Sertoli cells**

1369 1. Prepare Erlenmeyer flask by adding:

1370 a. Trypsin, 10x (2.5 x W_T) = _____mL

1371 b. DPBS (22.5 x W_T) = _____mL

1372 c. DNaseI (100 x W_T)= _____µL (Start with 100 µL of DNAse1 and then added 1

1373 mL at the 20 min mark and another 1 mL at the 25 min mark.)

1374 DNaseI is very critical, always favor more rather than less and be certain about the

1375 concentration when preparing the stock. This along with the flask could be why you

1376 are having clumping problems.

1377 Before adding tissue place in a clean petri dish and using a clean razor blade chop downward

1378 across the tissue and then rotate the plate 90° and chop across the tissue again until the tissue

1379 loses its grape structure as a pre-processing step to help break up the tubules so they digest

1380 easily.

1381 Add tissue to the flask. Cover flask with foil, incubate at 37°C for 25-30 min, with occasional

1382 swirling. During the last ten minutes, tissue should come apart rapidly. If after 20 min strings

1383 seen while swirling (this is very empirical when properly digesting the tissue will break up into

1384 pieces approx 2-3 mm in length and be independent of each other not clumped together), add
1385 DNaseI at (50 x W_T _____µL), after an additional 5 min add DNaseI at (25 x W_T _____µL).

1386

1387 2. When tubules are separated, move flask to sterile hood, let tubules settle for 5 mins. Then
1388 remove and discard overlying liquid. The solution will be very sticky and the tissue will want
1389 to come out with the supernatant. Don't lose too many cells here, if you can not get all the
1390 supernatant off just go ahead and add the trypsin inhibitor, but use another 0.5 mL on top
1391 of what you have figured to compensate for the increased volume.
1392 3. Add trypsin inhibitor (2.5 x W_T)=_____ mL. Swirl and incubate for 1 min.
1393 4. Add (25 x W_T) =_____ mL fresh DPBS, swirl, allow to settle. (Wait to add this if you did not
1394 get much of the supernatant off before, too much volume will increase the buoyancy and
1395 not let the cells settle out.
1396 5. Remove supernatant, add (20 x W_T)=_____ mL DPBS, swirl,
1397 allow to settle.

1398 6. Remove supernatant, add
1399 a. (7.5 x W_T)=_____mL DPBS
1400 b. Collagenase (2.5 x W_T)=_____ mL
1401 c. DNaseI (25 x W_T)=_____ µL (Add in 1mL here of DNaseI instead if
1402 below 1 mL)

1403 7. Incubate in water bath at 37°C for 10 min. After 5 min, swirl continuously. (During the last 3
1404 min aliquots are checked by microscope to monitor the release of peritubular cells. A drop
1405 of suspension is placed on a glass slide and the tissue is viewed under a coverslip at 10x

1406 mag. The coverslip is moved slightly and as the tissue moves peritubular cells can be seen to
1407 peel off. The tissue is very fragile at this stage and must not be allowed to over digest.
1408 Digestion is complete when the surface of large fragments no longer appears smooth.

1409 8. Transfer tubules to 50 mL conical tube, wash the flask with DPBS, and centrifuge at 200xg
1410 for 2 min.

1411 9. Remove supernatant, add 30-35 mL DPBS, and centrifuge again.

1412 10. Repeat step 9.

1413 11. Remove supernatant and resuspend and plate cells in Sertoli cell media containing retinoic
1414 acid from ScienCell™.

1415 12. Cells are incubated at 37°C in 5% CO_2, in a humidified chamber. Medium is changed every 48
1416 hours after 24-36 hours shock the cells with 10 mM Tris-HCl, pH 7.4 for 2 min. This will
1417 remove most of the contaminating germ cells. Make this media by dissolving 12.1g of
1418 Trisbase in 80 mL of ddH_2O and adjust the pH to 7.4 with HCl. This will make a 1M stock. To
1419 make a 10 mM solution, add 1mL of this 1M stock to 99 mL of ddH_2O and filter sterilize.

1420

1421 **Supplementary file 1h.**

1422 **Preparation of primary cultures of granulosa cells from mice protocol**

1423 **Materials:**

1424 70% EtOH	(Fisher: Cat. No. BP8203)
1425 500 mL DPBS	(Thermo Fisher: Cat. No. 14040133)
1426 BSA	(Sigma: Cat. No. A9085)
1427 Collagenase type IV	(Worthinton: Cat. No. LS004188)
1428 Glass Pipettes	(Fisher: Cat. No. 13-678-20A)
1429 DMEM/F12	(Gibco Cat. No. 21041-025)
1430 FBS	(Gibco Cat. No. 10082-147)
1431 Penicillin/Streptomycin 100X	(Gibco Cat. No. 15140-122)
1432 0.25% Trypsin-EDTA	(Gibco Cat. No. 25200-072)

1433 **Procedure:**

1434 A. **Preparation of media**

1435 1. Prepare 50 mL of DPBS with 0.5% BSA by dissolving 0.25 g of lyophilized BSA powder into 50
1436 ml of DPBS medium.
1437 2. Collagenase type IV solution (540 U/pair of ovaries) in 3 mL of DPBS.
1438 3. Prepare a glass pipette with a pointed tip that you can use to transfer the follicles. Set up an
1439 alcohol flame. Holding a glass pipette from both ends place the thicker section of glass just
1440 before the pipette tapers off over the hottest part of the flame. Rotate the tubing to make

1441 sure it is evenly heated. Continue to heat the glass until it starts to melt and becomes
1442 flexible. Then, with a quick motion, pull the glass so it forms a thin tube section. This will
1443 take some trial-and-error force that will give you the size that works best. Etch the glass and
1444 tap near the etched section to make a clean break in the tube. Finally, sterilize the tube and
1445 remove jagged edges by quickly running the completed tube through the flame. Attach the
1446 glass pipette to some form of controlled suctioning device (i.e. tubing connected to small
1447 syringe)
1448
1449 4. Prepare 50 mL of DMEM/F12 with 15% FBS by adding 7.5 mL of FBS and 0.25 mL of 100X
1450 Penicillin/Streptomycin stock solution to 42.25 mL of DMEM/F12 medium.
1451

1452 B. **Isolation of ovarian follicles from mice**

1453 1. Sacrifice mice by CO_2.
1454 2. Wipe down abdomen with 70% EtOH.
1455 3. Make abdominal incision.
1456 4. Remove the ovaries and immerse in DPBS in petri dish.
1457 5. Decap the ovaries by resecting away fat and connective membranes that surrounds and
1458 protect the ovary.
1459 6. Transfer the decapped ovaries to a clean petri dish with DPBS and no BSA. This will help to
1460 clean off any contaminating hairs, or fat and blood droplets released while decapping the
1461 ovaries.
1462 7. Section the ovaries into fourths by cutting them with the needle and forceps. This will help
1463 the collagenase digest the tissue and release follicles in the next step.

1464 8. After the ovaries have been divided into fragments add them to the activated
1465 collagenase digest solution and let the ovaries digest for 25 mins under constant
1466 agitation.
1467 9. At the end of 25 mins add in DPBS containing 0.5% BSA to inactivate the collagenase then
1468 centrifuge the tube at 60xg for 5 mins to pellet the follicles[214].
1469 10. After the tissue digest has finished spinning remove the supernatant and resuspend in 7 mL
1470 of DPBS with 0.5% BSA and transfer to a new petri dish to individually pick out follicles.
1471

1472 C. **Preparation of granulosa cells**

1473 1. Take the petri dish containing resuspended ovarian tissue and place it under
1474 stereomicroscope.
1475 2. Move the preantral follicles over to the clean droplet of DPBS with 0.5% BSA. It's best to
1476 move only a few follicles over at a time as pulling up many follicles can cause them to
1477 sediment and stick to the inside of the glass pipette if they are pulled up too far inside.
1478 3. Once you have moved over enough follicles, set up a 1.5 mL microcentrifuge tube containing
1479 1 mL of 0.25% activated trypsin.
1480 4. Gently swirl the dish containing the preantral follicles to get them to clump together in the
1481 center and collect them with a 1000 µL micropipette before transferring them to the droplet
1482 containing the trypsin EDTA.
1483 5. Let the follicles digest for 5 minutes. Pipette the digesting cells to help break up the follicles
1484 during the incubation period.
1485 6. Spin tube at 1000xg for 5 mins to pellet the granulosa and oocyte cells.
1486 7. Remove the supernatant and resuspend pellet in DMEM/F12 supplemented with 15% FBS
1487 and plate cells.

Supplementary file 1i.

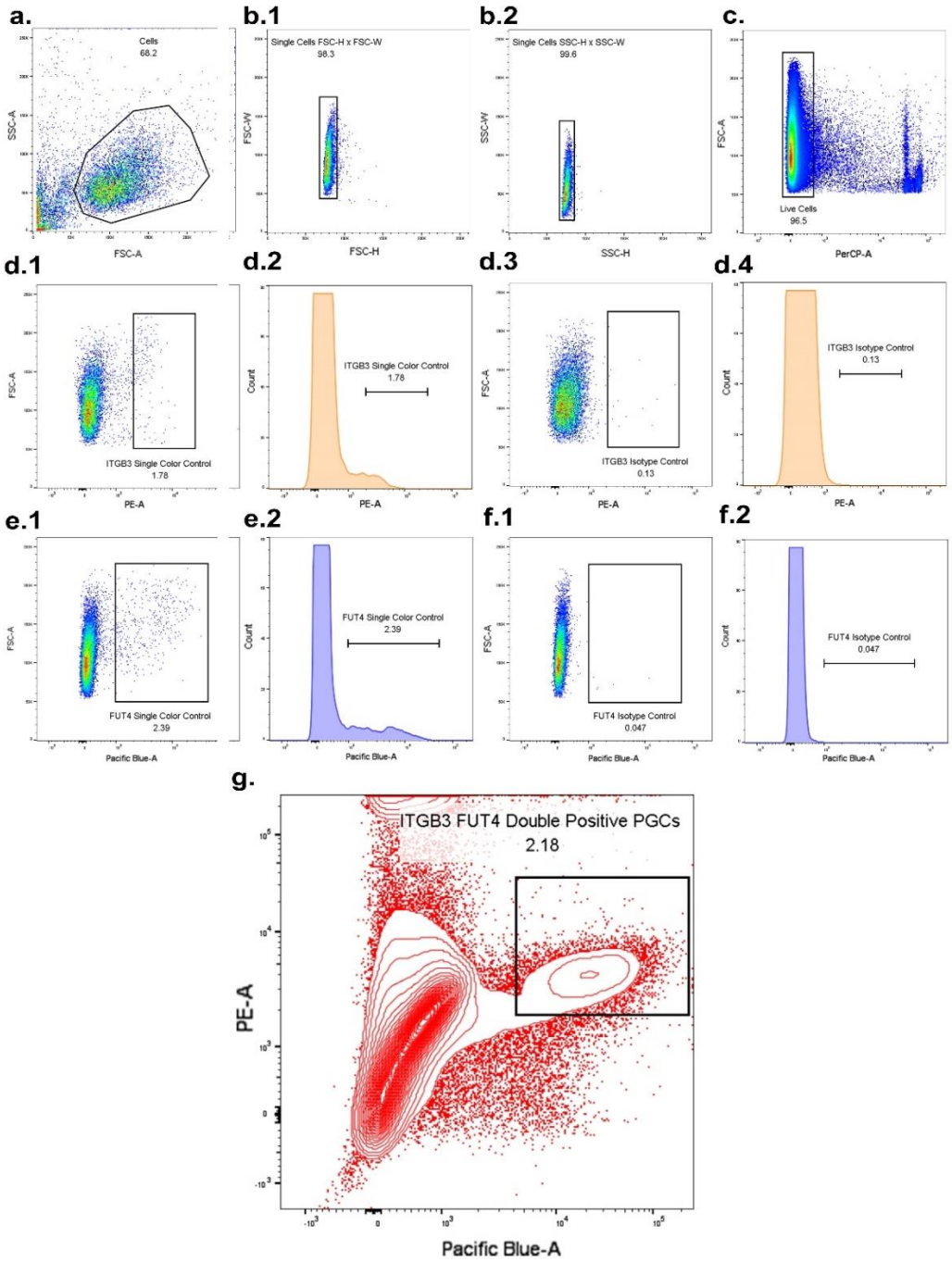

Supplement figure 5. FACS sorting for ITGB3/FUT4 enriched primordial germ cell like cells. a) Gating for cells. **b.1-2)** Gating for singlet cells. **c)** Gating for live cells. **d.1-2)** Single color control ITGB3 positive cells. **d.3-4)** IgG isotype control. **e.1-2)** Single color control FUT4 positive cells. **f.3-4)** IgG isotype control. **g)** Sorting for PGCLC-enriched ITGB3/FUT4 double positive population (2.18% of total cells)

Supplementary file 1j.

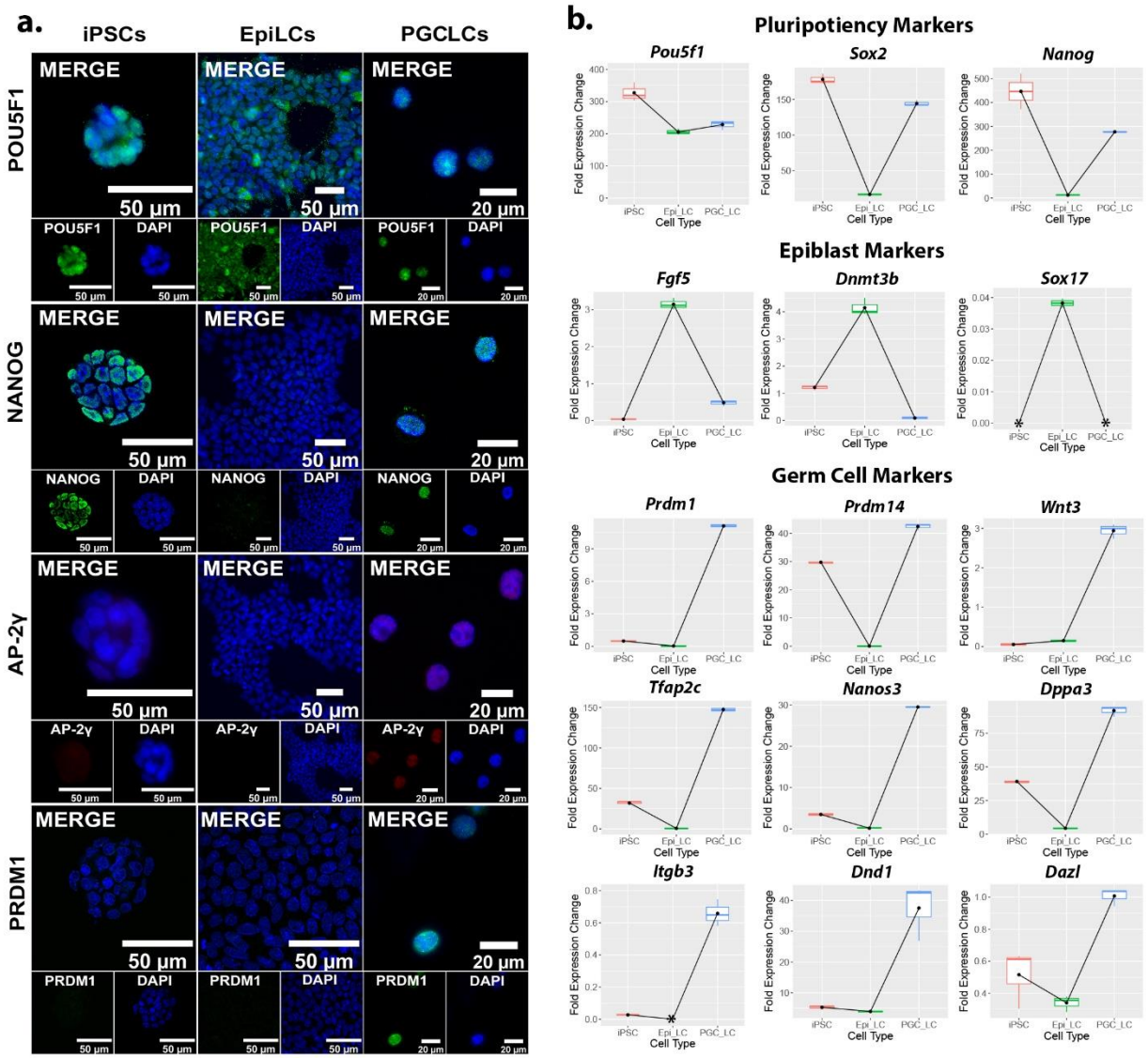

Supplement figure 6. Relative expression of markers for PGCLC induction from iPSCs. a) ICC of pluripotency and germ cell marker expression throughout the transition from iPSCs to PGCLCs. **b)** qRT-PCR of pluripotency, epiblast, & germ cell markers indicating gene expression profiles during induction of PGCLCs from iPSCs. Each gene fold expression is relative to the housekeeping gene *Gusb* using the ΔCq method. The symbol * indicates that the expression of transcripts in the sample were either non-existent or so low as to be undetectable by qRT-PCR.

1503 **Supplement table 9. Primer designs**

Gene	Forward	Reverse	Efficiency
Pou5f1	TTCAGCCAGACCACCATCTGT	GGTTCTCATTGTTGTCGGCTTC	106.02%
Nanog	GTGCTTGCTTGTCCTTGGAG	AGCTGGCATCGGTTCATCAT	103.86%
Tfap2c	AGGCATCTCATTTCTGCGGG	CACGGACAGGCTTAGAGGTC	101.37%
Prdm1	GAAAAATGGGAGCCCCGACA	AAGACGGAAGGGGACTGTGA	92.60%
Prdm14	ACAGCCAAGCAATTTGCACTAC	TTACCTGGCATTTTCATTGCTC	104.57%
Sox2	TTGGGAGGGGTGCAAAAAGA	TTCTAGTCGGCATCACGGTT	98.20%
Sox17	CAAAGCGAAGATTGCAGGGT	TTTCCAGTCCCTGGTCAGTC	107.78%
Fgf5	TACGTGGCCCTGAACAAGAG	TGGAACAGTGACGGTGAAGG	108.72%
Dnmt3b	GCTTTGCTTCACTGGGTCTC	AACTGATGGGGTACTGACGC	98.12%
Wnt3	CCTGGACCACATGCACCTAAA	CGGAGGCACTGTCGTACTTG	95.11%
Nanos3	CACTACGGCCTAGGAGCTTGG	TGATCGCTGACAAGACTGTGG	90.56%
Dppa3	TGAACGGGACAGTGAGCCA	AGCCAGGGCAGCGTACAAT	99.12%
Itgb3	ACGGGACTTTTGAGTGTGGG	GCTGAGAGGGTCGGTAATCC	100.54%
Dnd1	AATGGGTTAAGCAGAGCCTGT	AGGGCAAGGTTCCTCACAAC	96.18%
Dazl	GCAGAGAACCTTTGTACCCAC	TAGCAAGGTGCTGTTCCAGTG	102.75%
Gusb	GCAGCCCTTCGGGACTTTAT	TCCTCAACACCACTCTCATGTC	97.17%

1504

1505

1506

Supplementary file 1k

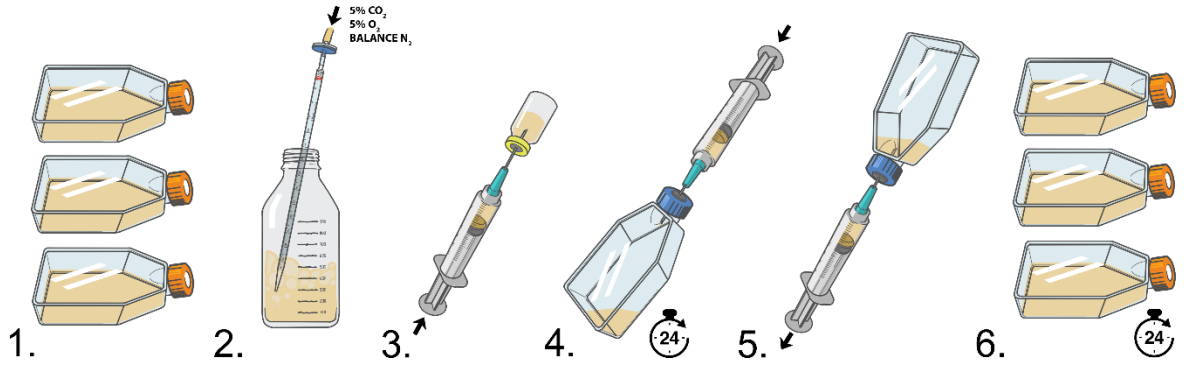

Supplement figure 7. Chemical exposure experimental workflow. 1) Cells are passaged into T-25 flasks with filter caps. **2)** Mixed blood gas (carbon dioxide 5%, oxygen 5%, and balance nitrogen) is filtered and bubbled into media to prepare media to be mixed with diluted chemical treatment and added to air-tight cell culture flasks. **3)** Media is transferred into glass vials and diluted chemical is added. **4)** T-25 filter caps are replaced with air-tight caps with septums and cell media containing chemicals is added via syringe and left for 24 hours. **5)** After 24 hours, chemical-containing media is removed and cells are washed with buffer. **6)** T-25 air-tight septum caps are replaced with filter caps and cells are cultured for an additional 24-hour “chase” period.

Supplementary file 1m.

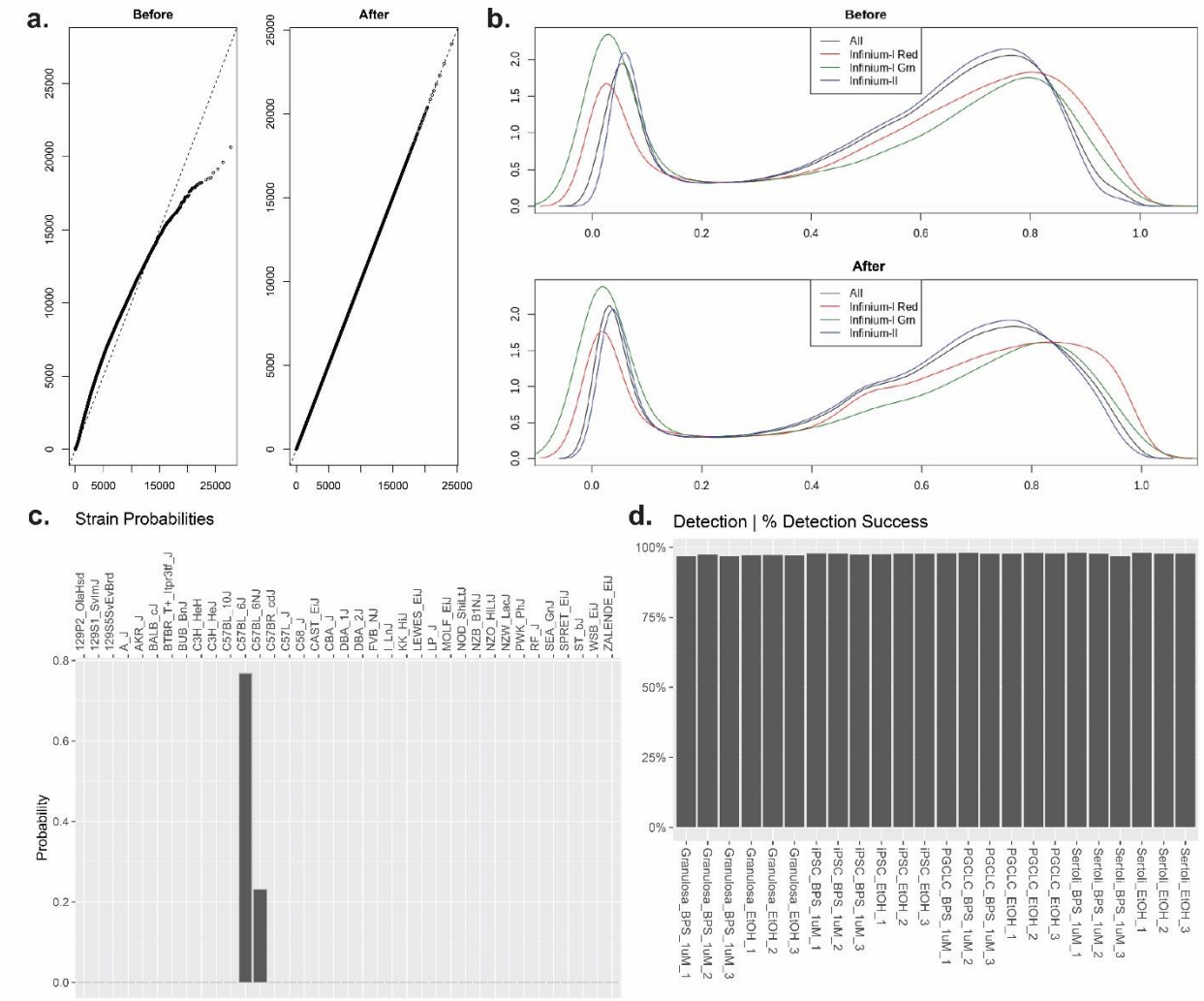

Supplement figure 8. Quality control for Infinium Mouse Methylation BeadChip Array data. a) Non-linear correction of dye bias removal from sample data. **b)** Background signal subtraction from samples to limit noise. **c)** Prediction of correct C57B6 mouse strain from samples included in the study based on built-in controls on Infinium Mouse Methylation BeadChip Array. **d)** Average CpG probe detection success of 97.58% percent across all samples indicating efficient bisulfite conversion of all samples.

Supplementary file 1n.

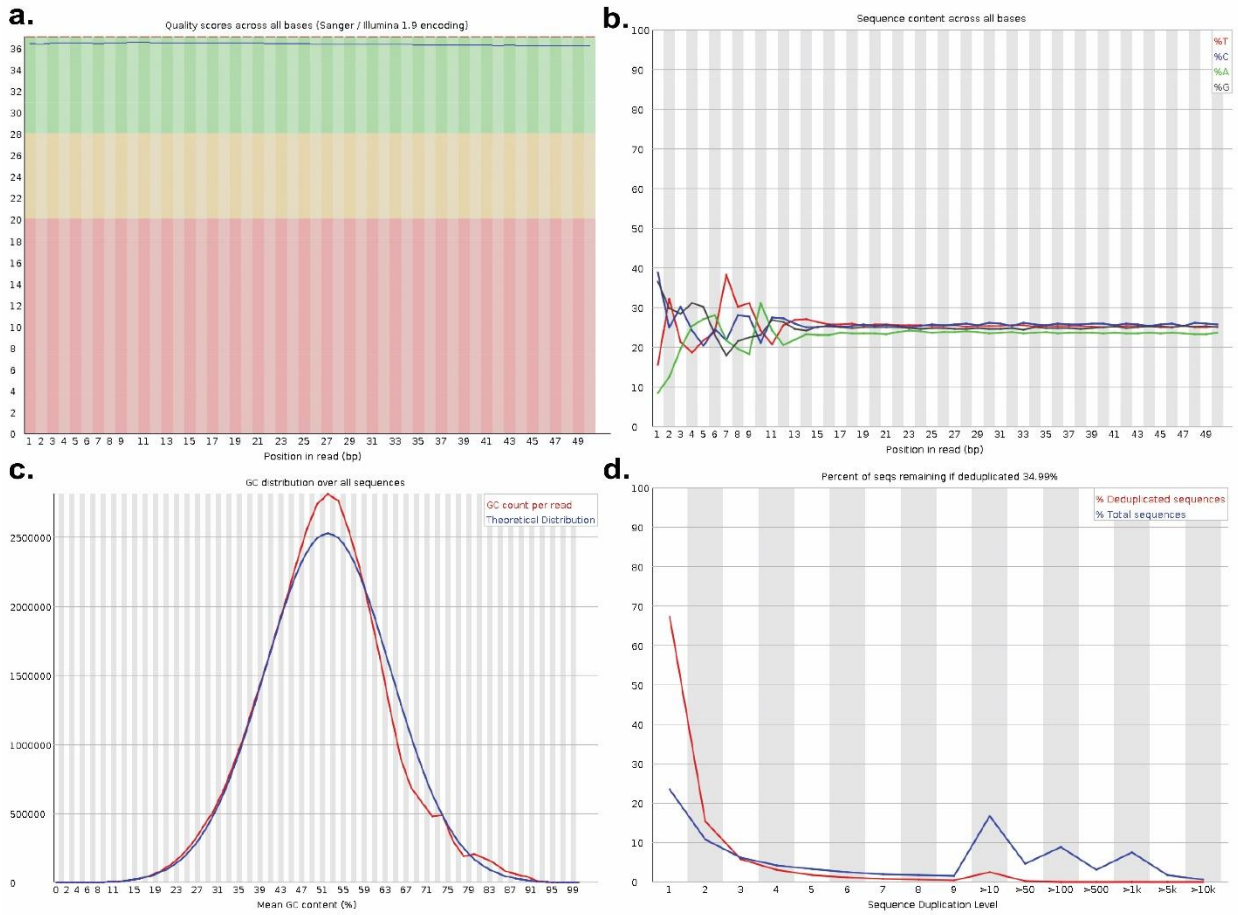

Supplement figure 9. Quality control for RNA-seq data. RNA-seq quality control data from a one of the three PGCLC replicates exposed to BPS as an exemplar **a)** Base calls had high quality scores (phred scores > 30) for all bases in reads. **b)** Reads showed equal distributions of all four bases following the initial adaptor sequence and sufficient base complexity. **c)** Distribution of GC sequences across reads aligns very closely with the theoretical distribution. **d)** Duplication plot indicates deduplicated libraries contained ~67% unique sequences which indicates sufficient library complexity for subsequent downstream data processing.

1540 **Supplementary file 1o**

1541 **Supplement table 10. Quality control metrics for EM-seq data.**

Sample	Insert Size (bp)	Median Coverage	Read Counts (Millions)	Aligned Reads (%)	Duplicate Reads (%)	GC (%)
iPSC_E_1	320	37 X	851.9	99.0	28.6	22
iPSC_E_2	374	33 X	752.6	99.1	26.4	22
iPSC_E_3	378	38 X	873.5	99.2	27.2	22
iPSC_BPS_1	360	28 X	626.7	99.1	23.6	22
iPSC_BPS_2	330	30 X	695.3	99.1	26.6	22
iPSC_BPS_3	338	33 X	755.8	99.1	27.7	22
PGCLC_E_1	388	32 X	707.9	99.0	25.6	23
PGCLC_E_2	374	25 X	559.4	99.0	24.0	22
PGCLC_E_3	412	30 X	673.5	99.2	24.9	22
PGCLC_BPS_1	399	31 X	672.9	99.1	25.6	22
PGCLC_BPS_2	371	32 X	753.3	99.1	28.6	22
PGCLC_BPS_3	392	27 X	599.3	99.1	23.6	22

1542

1543